AIAA 95-0863

Comparative Numerical Testing of One- and Two-Equation Turbulence Models for Flows with Separation and Reattachement

M.Shur, M.Strelets, and L.Zaikov
Federal Scientific Center "Applied Chemistry"
St.-Petersburg 197198, Russia
and
A.Gulyaev, V.Kozlov, and A.Secundov
Central Institute of Aviation Motors
Moscow 111250, Russia

33rd Aerospace Sciences Meeting and Exhibit
January 9-12, 1995 / Reno, NV

COMPARATIVE NUMERICAL TESTING OF ONE- AND TWO-EQUATION TURBULENCE MODELS FOR FLOWS WITH SEPARATION AND REATTACHMENT

M.Shur*, M.Strelets†, and L.Zaikov‡
Federal Scientific Center "Applied Chemistry", Saint-Petersburg, Russia
and
A.Gulyaev‡, V.Kozlov*, and A.Secundov†
Central Institute of Aviation Motors, Moscow, Russia

Abstract

Numerical testing of three recently proposed turbulence models proposed recently by Secundov and co-workers [1], by Spalart and Allmaras [2], and by Menter [3] is carried out for the 2D backward/forward-facing step benchmark flows that were studied experimentally in [4-7] and involved a wide range of Reynolds number, opposite wall angle, and step geometry. A grid refinement study is carried out for all the models and test cases to make sure that grid-independent results are obtained. On the basis of detailed comparison of the numerical results with the experimental data and also with similar results obtained in the framework of the well-known low Reynolds number k-ε model by Chien [8], the strengths and weaknesses of each model are found out.

1. Introduction

Debates about the optimal number of transport equations that should be involved in a turbulence model aimed for CFD engineering applications already have a long history. In the late eighties it seemed that finally the answer was found due to the impressive results that have been reached by an extensive use of the two-equation turbulence models, namely, the k-ε, k-ω, and similar ones. However, recently a lot of criticism was addressed to these models (primarily the k-ε model, which is in much wider use), associated with both their physical and computational shortcomings found out via intensive testing performed by numerous authors around the world and, especially, in the framework of the Collaborative Testing of Turbulence Models (CTTM) [9]. In particular, the most important physical drawbacks of the *so called low Reynolds number forms of the* k-ε model are their inability to predict consistently the near wall turbulent flows in the presence of strong adverse pressure gradients, and those with separation and reattachment (we leave *aside the models using wall functions since they* lose any justification for the flows with separation). As to the computational drawbacks of these models, they are well known and associated with a stiffness of the governing equations (it causes a significant degradation of the convergence to a steady-state), with the necessity to use very fine grids near a solid wall, and also with non-trivial inlet and freestream boundary conditions for the turbulence variables.

Perhaps, exactly these circumstances have provided for a strong motivation for a further development of the transport-equation *turbulence models and, in particular, have* reawaken the interest to the one-equation turbulence models being an attractive intermediate between the conventional algebraic and two-equation models. It resulted in the invention of new two- and one-equation turbulence models which seem to be very promising for a lot of aerodynamic applications. Three such models, two being one-equation [1,2] and one - a two-equation model [3], are chosen in this work for a detailed assessment from the standpoint of their capability of predicting the turbulent flows with massive separation and reattachment and with adverse pressure gradient, i.e., with the major hydrodynamics elements that prove difficult to predict using the conventional k-ε turbulence models.

The first of these models, the so called ν_t-92 model (its previous version is known as ν_t-90), was developed by Gulyaev, Kozlov &

---

* Senior Research Scientist

† Principal Scientist

‡ Research Scientist

Secundov [1]. It contains only one transport equation for the eddy viscosity ν_t and originates from the Kovasznay model [10, 11], but differs from the latter a lot by near-wall, compressibility and some other corrections. It is used intensively in Russia for the simulation of a wide range of industrial and aerodynamic flows. This model was entered in the CTTM [9] and turned out to be quite competitive for the turbulent boundary layers, mixing layers, plane and round jets, and plane and round wakes, but till now it has not been applied for the more complicated "elliptic" flowfields.

The second model we have chosen for evaluation was proposed not long ago by Spalart & Allmaras [2, 18]. It is also a one-equation ν_t-transport model and in this sense it is similar to the model [1]. However it arises from somewhat different prerequisites and so differs tangibly from the latter model.

The last model being considered in the present work is the so called Shear Stress Transport k-ω model by Menter [3]. It contains two transport equations, one written for the turbulence kinetic energy k and another for the specific dissipation rate ω. These equations are obtained from the standard k-ε model reformulated in the terms of k and ω and then coupled with the Wilcox k-ω model [12] by a special blend function. The latter is designed in such a way that the k-ε model governs mainly in the outer part of the flow and the k-ω in the inner, near-wall, part. Therefore each model is used in the region where it is known to be more successful and thus the combined model has a chance to posses their best features.

The Spalart-Allmaras (S-A) and Menter (M-SST) models have a lot of attractive properties from both accuracy and computational robustness viewpoints. Unlike the ν_t-92 model, the S-A and M-SST ones have been already used not only for the relatively simple "parabolic" flows, but also for rather complicated flowfields including the multi-element airfoil flows [13], and demonstrated very impressive capabilities. However, as far as the authors are aware, except maybe for the M-SST model no comprehensive studies of these models have been performed for now for the flows with massive separation and reattachment.

Exactly for this reason the sample problems that were chosen for a detailed assessment of the above turbulence models included the backward-facing step (BFS) flows which were thoroughly studied experimentally by Driver & Seegmiller [4] and by Jovic & Driver [5, 6]. These experiments cover a wide range of the opposite wall angles [4] and Reynolds number [5, 6] and hence provide enough background for an objective evaluation of the turbulence models performance as applied to such a flowfield.

Another benchmark flow whose distinctive feature is the presence of two recirculation zones is the forward-facing step (FFS) flow. The specific flowfield of such a type chosen in the present work for testing the turbulence models was that investigated experimentally by Moss & Baker [7].

Since the ν_t-92 model is still virtually unknown to the Western Fluid Dynamics Community, in the first part of the paper (Section 2) this model is described in some detail along with the results illustrating its capability of predicting the conventional parabolic benchmark flows. In Section 3, devoted to the comparative study of different turbulence models performance as applied to the backward- and forward-facing step flows, we first shortly dwell upon the flow solver used for these flow simulations, then the results of the grid refinement study are discussed and, finally, the results obtained for the BFS and FFS flows on the basis of different turbulence models are presented.

2. ν_t-92 Turbulence Model

The current state of this model is a result of numerous improvements of the Kovasznay turbulence model [10, 11] that have been carried out for more than twenty years by Secundov and his co-workers.

In 1971 [14] they succeeded in making the original model [10] really closed by establishing a relation between the turbulence scale that was involved in the Kovasznay eddy viscosity transport equation and the distance to the wall. Some enhancements of the model were then performed in 1975 which improved its performance as applied to jet flows with account of the compressibility effects [15] and to the boundary layer flows with account of the wall roughness [16]. In 1986 [17] some additional compressibility corrections were included in the eddy viscosity transport equation. This, the first, stage of the work on the model resulted in the development of its version known as the ν_t-90 model. As mentioned in the Introduction, it was entered in the CTTM and turned out to be quite competitive for a wide range of 2D parabolic flows. On the other hand, the CTTM and subsequent discussions with Dr.Spalart (who, in particular, drew the authors' attention to the *non-invariance of the ν_t-90 model to coordinate* transformation), have highlighted weak sides of this model, leading to the development of its improved current version ν_t-92 [1].

Let us consider some specific features of this model in more detail.

2.1. Description of the Model.

Just as the original Kovasznay model [10] it contains only one transport equation formulated directly for the eddy viscosity ν_t. In the framework of the ν_t-92 model this equation reads as follows:

$$\frac{\partial\rho\nu_t}{\partial t}+\frac{\partial\rho u_i\nu_t}{\partial x_i}=\frac{\partial}{\partial x_i}\left[\rho\left(C_0\nu_t+\nu\right)\frac{\partial\nu_t}{\partial x_i}\right]+ +\frac{\partial}{\partial x_i}\left\{\rho\left[\left(C_1-C_0\right)\nu_t-\nu\right]\right\}\frac{\partial\nu_t}{\partial x_i}+P_\nu-D_\nu \tag{1}$$

where u_i are the mass-weighted (Favre) averaged velocity components, ν is the molecular (laminar) kinematic viscosity, and P_ν and D_ν are the production and dissipation terms defined as follows:

$$\begin{aligned}P_\nu-D_\nu={}&\rho C_2F_2\left(\nu_t\Gamma_1+A_1\nu_t^{4/3}\Gamma_2^{2/3}\right)+\\&+\rho C_2F_2A_2N_1\sqrt{\left(\nu+\nu_t\right)\Gamma_1}-\rho C_5\nu_t^2\Gamma_1^2/a^2+\\&+\rho C_3\nu_t\left(\frac{\partial^2\nu_t}{\partial x_i\partial x_i}+N_2\right)-\\&-\rho C_4\nu_t\left(\frac{\partial\langle U_i\rangle}{\partial x_i}+\left|\frac{\partial\langle U_i\rangle}{\partial x_i}\right|\right)-\\&-\rho\left[C_6\nu_t\left(N_1d_w+\nu_w\right)+C_7F_1\nu\nu_t\right]/d^2\,.\end{aligned} \tag{2}$$

Here a is the speed of sound, d is the distance to the closest wall, modified to account for the effect of wall roughness:

$$d=d_w+0.01k_s\,, \tag{3}$$

where d_w is the "real" distance to the wall and k_s is the roughness height.

The functions F_1 and F_2 are given by

$$F_1=\left(N_1d_w+0.4C_8\nu\right)/\left(\nu_t+C_8\nu+\nu_w\right), \tag{4}$$

$$F_2=\left(\chi^2+1.3\chi+0.2\right)/\left(\chi^2-1.3\chi+1.0\right), \tag{5}$$

$$\chi=\nu_t/(7\nu)\,, \tag{6}$$

with ν_w being the ν_t value at the wall, equal to zero at a smooth wall, and the quantities Γ_1, Γ_2, N_1 and N_2 being as follows:

$$\Gamma_1^2=\frac{\partial u_i}{\partial x_j}\left(\frac{\partial u_i}{\partial x_j}+\frac{\partial u_j}{\partial x_i}\right), \tag{7}$$

$$\Gamma_2^2=\sum_i\left(\frac{\partial^2u_i}{\partial x_j\partial x_j}\right)^2, \tag{8}$$

$$N_1^2=\sum_i\left(\frac{\partial\nu_t}{\partial x_i}\right)^2, \tag{9}$$

$$N_2^2=\sum_i\left(\frac{\partial N_1}{\partial x_i}\right)^2. \tag{10}$$

The constants of the model are given by:

$$\begin{gathered}A_1=-0.5,\quad A_2=4.0,\\C_0=0.8,\ C_1=1.6,\ C_2=0.1,\ C_3=4.0,\\C_4=0.35,\ C_5=3.5,\ C_6=2.9,\ C_7=31.5,\ C_8=0.1.\end{gathered} \tag{11}$$

The essential differences of equation (1) from its previous versions mentioned above, as well as from the similar equations proposed recently by Spalart and Allmaras [2, 18], are associated with the following additional terms:

$$\rho C_2F_2\left[A_1\nu_t^{4/3}\Gamma_2^{2/3}+A_2N_1\sqrt{\left(\nu_t+\nu\right)\Gamma_1}\right]+ +\rho C_3\nu_t\left(\frac{\partial^2\nu_t}{\partial x_i\partial x_i}+N_2\right). \tag{12}$$

The physical reasons for including these terms into the eddy viscosity transport equation were as follows.

First, the results of the simulations of the mixing layers performed on the basis of various turbulence models show the necessity of increasing the generation terms in the ν_t transport equation for a better correspondence between the predicted and measured eddy viscosities. Exactly for this reason the combination $\Gamma_1^{1/2} N_1$ was added (note that the eddy viscosity transport equation proposed in [2, 18] also contains a term with N_1).

Second, though there is no direct substantiation of the impact of the second-order velocity derivative Γ_2 on the ν_t generation, some circumstantial evidence of such an impact does exist. In a number of studies an interaction was observed between the shear flow stability, characterized by the amplification of small disturbances, and the turbulence. Under the favorable longitudinal pressure gradient the velocity profile in the boundary layer is more convex than that in a flat plate boundary layer, i.e., the value of Γ_2 in the former case is higher than in the latter one.

Since the more convex profile is known to be more stable, it gets clear that some term containing Γ_2 should be introduced into the model equation, presumably with a small negative factor.

Finally, the motivation for adding the terms $\partial^2\nu_t/(\partial x_i \partial x_i)$ and N_2 is the desire to describe more precisely the axisymmetric flows. It is well known [19] that they differ essentially from the plane ones by the large-scale vortical structure. In particular, in the plane jets the asymmetrical mode of the oscillations does prevail, while in the axisymmetric jets the first azimuthal mode is more significant. Thus it seemed to be important to find a dimensionless criterion to associate with the specific features of the axisymmetric flows. In the ν_t-92 model such a criterion, Q, is based on the measure of nonuniformity of the eddy viscosity field, i.e., $Q = \nu_t(\Delta\nu_t + N_2)/N_1^2$. As a rule, the ν_t profile in a plane shear flow is convex, therefore $\Delta\nu_t$ is negative and Q is close to zero. In the axisymmetric flows with similar distributions of the parameters, Q is proportional to $-\nu_t/(N_1 r)$ and so it is negative. Besides, for both plane and axisymmetric cases this term provides for "straightening" of the eddy viscosity profile near the boundary of the turbulent fluid, i.e., makes its distribution in that region close to linear one.

The compressibility effects are described in the ν_t-92 model by means of the following two terms in the eddy viscosity transport equation (1):

$$- \rho C_4 \nu_t \left(\frac{\partial \langle U_i \rangle}{\partial x_i} + \left| \frac{\partial \langle U_i \rangle}{\partial x_i} \right| \right) - \rho C_5 \nu_t^2 \Gamma_1^2 / a^2 \qquad (13)$$

The first term, containing the divergence of the time (Reynolds) averaged velocity, is responsible for the turbulence generation due to the mean velocity divergence and for the work of the buoyancy forces [15, 17]. It is designed in the form which provides for proper prediction of both the strong decrease of the eddy viscosity in the Prandtl-Mayer flow and the relatively slight change of that in the shock waves [20]. This term can also play some, though a minor, role in the subsonic flows with a heat release (the calculations of the subsonic combustion performed on the basis of the ν_t-92 model in [21] has shown that the impact of this term for such flows does not exceed 10-20%).

In order to evaluate the value of the Reynolds-averaged velocity divergence in (13) the continuity equation and an appropriate approximation for the correlation $\langle \rho' u_i' \rangle$ should be used, which results in the following relation:

$$div\langle \vec{U} \rangle \cong div\,\vec{u} + div\left(\frac{\nu_t}{\rho \Pr_t} \cdot grad\,\rho \right) \qquad (14)$$

The second term in (13) is responsible for the work of compression and hence can play a considerable role only in supersonic flows.

As it was mentioned the effect of the wall roughness k_s on the eddy viscosity is accounted for in the ν_t-92 model by the treatment of the distance to the wall *d* in the near-wall destruction terms in accordance with the relation (3) [16]. It is, in fact, nothing else than the conventional "shift" of the wall-normal coordinate used in the Prandtl mixing length theory for the boundary layer on a rough wall. Besides, for the case of rough surface the conventional wall boundary condition for the eddy viscosity $(\nu_t)_w = 0$ is replaced by the following one:

$$\left(\nu_t\right)_w = 0.02\,\nu^* k_s \qquad (15)$$

with the friction velocity ν^* being defined as

$$\nu^* = \sqrt{\tau_w / \rho}.$$

2.2. Some Previous Results of the ν_t-92 Model Validation

The capabilities of the ν_t-92 turbulence model outlined above have been evaluated on a wide set of benchmark problems including the following: boundary layer on both smooth and rough flat plate at Mach number ranging from zero (incompressible flow) to 10 and momentum thickness Reynolds number ranging from 100 to 20000; self-similar plane mixing layer formed by a uniform flow in still air at Mach number ranging from zero to 20; round and plane jets in still air; homogeneous shear flow; self-similar wakes of a sphere, cylinder, cigar shaped streamlined body and plane wing. This evaluation has shown that the ν_t-92 model is tangibly more universal (applicable to a wider range of flow conditions) than its previous version ν_t-90. As a substantiation, some results are presented below, obtained for the boundary layers and jets on the basis of the ν_t-92 model.

Boundary Layer on a Flat Plate. The velocity profiles for this flow calculated at different momentum thickness Reynolds numbers (Re_{th}) are presented in Fig.1. By the dashed line the following velocity profile [9]

$$U / \nu^* = (1/K)\ln\left(y^+\right) + C,\; y^+ = y\nu^* / \nu,$$
$$K = 0.41, \quad C = 5. \qquad (16)$$

is depicted which is regarded as the best approximation of the experimental data.

One can see that the correspondence between the predictions and the experimental data is fairly good for all the Re_{th} values.

Mixing Layer, Plane and Round Jet. The values of the main geometrical characteristics of these flows computed on the basis of both ν_t-90 and ν_t-92 models are presented in Table 1, along with the data suggested as the best ones in [9]. Appropriate mean velocity and eddy viscosity profiles for the mixing layer are plotted in Fig. 2.

Table 1. Comparison of ν_t-90 and ν_t-92 models predictions with experimental data

Problem	Suggested value	ν_t-90	ν_t-92
Mixing layer, db^*/dx [a]	0.115	0.125	0.108
Plane jet, $db_{0.5}/dx$ [b]	0.107	0.168	0.126
Round jet, $db_{0.5}/dx$	0.093	0.099	0.103

[a] mixing layer width defined as a distance between 0.1 U_{max} and 0.9 U_{max}

[b] jet half-width defined by $u(x,b_{0.5})=0.5\,u(x,0)$

It is clearly seen that the new version of the model provides for a tangibly better correspondence between the computed results and the experimental data for the plane jet than the previous one (recall that the poor prediction of the plane jet characteristics was precisely one of the reasons that stimulated the attempts to improve the ν_t-90 model). Nevertheless, the discrepancy still remains rather significant.

Boundary Layer on a Rough Solid Wall. It is quite obvious that the simple approach used in the ν_t-92 model in order to take into account the wall roughness can not claim to describe such subtle effects as the laminar/turbulent transition at a rough wall or the influence of the roughness type. Nevertheless, it turns out quite capable of predicting the wall roughness influence on the mean velocity profiles and wall friction at relatively high Reynolds number. This property of the model is illustrated by Fig.3.

Compressible Boundary Layer and Mixing Layer. Some results of the compressible boundary layer calculations are shown in Figs.4,5. One can see that the ν_t-92 model predicts a rather slight effect of the Mach number on the boundary layer velocity profile. At the same time the decrease of the skin friction coefficient with increasing Mach number is rather significant and, as it is shown in Fig.5, in a wide range of Mach number variation the predicted C_f values are virtually the same as the generalized experimental data used for the CTTM-90/91, due to Van Driest.

The results of the compressible mixing layer calculations are presented in Fig.6 together with the experimental data by different authors assembled by D. Papamoschou [22], M_c in this figure being the so called convective Mach number $M_c = (u_{min} + u_{max}) / (a_{min} + a_{max})$. The calculations are performed using the turbulent Prandtl number $Pr_t = 0.5$. Considering the significant disparity of the experimental data one can conclude that the performance of the ν_t-92 model as applied to this flow is quite acceptable.

3. Assessment of the V_t-92, S-A, and M-SST Models as Applied to the Backward/Forward-Facing Steps Turbulent Flows

In this Section we present the results of the comparative numerical study performed in order to evaluate the capability of the three turbulence models listed above to predict the backward- and forward-facing steps flowfields and to assess their advantages (disadvantages) over the conventional low Reynolds number *k*-ε *models, namely, the model proposed by Chien* [8] and known as one of the computationally most efficient low Re versions of the *k*-ε model.

3.1. Benchmark Backward/Forward-Facing Step Flow Description

The schematics of three flowfields chosen in this study as the benchmark problems for the *turbulence models testifying* are presented in Table 2. The first, backward-facing step flow, was studied experimentally by Driver & Seegmiller [4] (D & S flow). It is the flow in a diverging channel in which the wall opposite the step side can be deflected at different angles to *impose different pressure gradients* on the freestream. The data obtained by Driver & Seegmiller have been used as a test case in a

Table 2. Schematics and main parameters of the benchmark flows

	Driver & Seegmiller [4] Flow	Jovic & Driver [5,6] Flow	Moss & Baker [7] Flow
Flow schematic	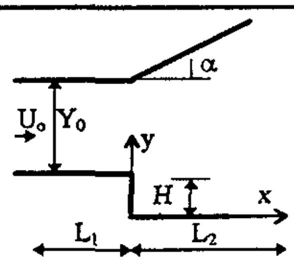	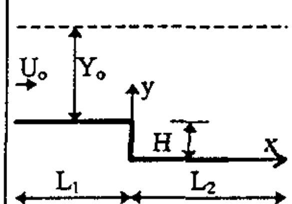	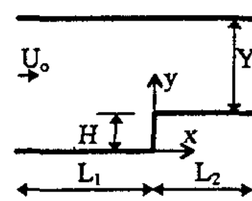
Step height, H (mm)	12.7	Case 1: 9.65 Case 3,4: 26.0	76.0
Freestream velocity, U_0 (m/s)	44.2	Case 1: 7.7 Case 3: 6.0 Case 4: 14.6	10.0
Opposite wall angle, α	-2° ÷ +8°	No opposite wall	0°
Reynolds number, Re_H	37500	Case 1: 5000 Case 3: 10400 Case 4: 25500	47740
Re_{th} at reference test section	5000 at x = -4.0H	Case 1: 610 at x=-3.05H Case 3: 1650 at x=-2.31H Case 4: 3600 at x=-2.31H	n/a
$\frac{Y_0}{H}; \frac{L_1}{H}; \frac{L_2}{H}$	8; 4; 32	Case 1: 5; 10; 20 Case 3,4: 7; 10; 20	10; 20; 20

lot of numerical studies, including the CTTM, in order to estimate the capabilities of different models to predict a reattachment of the separated shear layers in the presence of an adverse pressure gradient.

The second set of the experiments with the backward-facing step is that performed by Jovic & Driver [5, 6] (J & D flow). One of these flows (Case 1 in Table 2) was also studied numerically by Lee, Moin, and Kim [23] on the basis of the DNS technique.

As one can see from the Table 2, the J & D flow differs from the D & S one not only by the geometry (it is a plane channel with a symmetric sudden expansion) but also by the wide range of the Reynolds number variation.

As it was shown in [6] this parameter affects crucially the flow characteristics in the separation region. In particular, the maximum value of the negative shear stress in the J & D flow with Re = 5000 (Case 1) turns out to be about three times higher than that in the D & S experiments. Thus the comparison of the computed results with these two sets of the experimental data allows us, among other things, to evaluate whether the turbulence models being studied are able to predict such a sensitivity of the flow to the Reynolds number variation.

As far as the forward-facing step flowfield is concerned, it has been studied experimentally in much less depth than the backward-facing one. The only experimental data being complete enough to perform the corresponding numerical simulation we managed to find in the literature are those by Moss & Baker [7] (M & B flow), see Table 2.

The boundary conditions for the Navier-Stokes equations used in the present study for the numerical simulation of the flowfields described above are conventional ones. The only issue here is prescribing the appropriate inlet profiles of the flow parameters (u, ν_t, k and ω, or k and ε). In order to generate such profiles, first, the computations were performed of a flat plate boundary layer. Then the value of the momentum thickness Reynolds number Re_{th} for the velocity profile, prescribed as the inflow boundary condition, was chosen in order to match the experimental data on Re_{th} at the first test section, if the latter was known, or directly the corresponding velocity profile. Since the first experimental section, as a rule, is not located far enough upstream of the step, i.e., it falls in the region of its upstream influence, several iterations were usually performed in order to achieve a good match.

3.2. Flow Solver Description

For the numerical implementation of all the considered turbulence models we have used a two-dimensional Navier-Stokes solver based on the so-called Compressibility Scaling Approach [24, 25]. It presents one of the preconditioning methods eliminating the acoustic stiffness of the governing Navier-Stokes equations at low Mach numbers. Therefore this method can be used for an arbitrary Mach number flow including the incompressible flow limit ($M = 0$) without any degradation of the convergence to a steady-state typical for the conventional compressible Navier-Stokes algorithms. This property of the solver is crucial for the present work since all the flows being considered in this paper are virtually incompressible.

The finite-difference scheme used in the code is an implicit second order scheme of approximate factorization.

The convective terms in both the Navier-Stokes equations and the turbulence transport-equations are approximated by second order upwind differences and the terms with the pressure gradient by the corresponding downwind differences.

To prevent the oscillations associated with the switching of the scheme stencil at the points where the velocity of the flow changes its sign, the blended, central and upwind/downwind differences are used with the blend parameter being dependent upon the magnitude of the local velocity so that the central differences are introduced only in the vicinity of the points where the velocity is small. Finally, in order to prevent the odd-even pressure decoupling on the non-staggered grid system, artificial fourth order pressure dissipative terms are introduced into the continuity equation with the same blend parameter.

At every time step the continuity and momentum equations are solved by the block tri-diagonal matrix inversion algorithm, while the energy conservation equation and the transport equations for the turbulent variables (ν_t, k, ε, ω) are solved by the scalar tri-diagonal matrix inversions.

The finite-difference grids used in this study were obtained by the following simple coordinate transformation

$$\xi = f_1(\bar{x}), \quad \eta = f_2(\bar{y}), \tag{17}$$

Where ξ and η are the new, computational coordinates and $\bar{x}$ and $\bar{y}$ are the normalized physical coordinates

$$\bar{x} = \frac{x - x_{inl}}{x_{out} - x_{inl}}, \quad \bar{y} = \frac{y}{y_w}, \tag{18}$$

with x_{inl} and x_{out} being the coordinates of the computational domain inlet and outlet and y_w being the coordinate of the opposite wall for the D & S and M & B flows or of the symmetry plane for the J & D flow. As an example, the function f_2 used for the D & S flow simulation is plotted in Fig.7a. It is clearly seen that it provides grid clustering in the vicinity of the solid walls. For instance, for a grid with 120 nodes in y-direction for the D & S flow a ratio of the maximum and minimum y-steps is approximately 250, while the maximum ratio between neighboring y-steps is 1.19. For the J&D flow and the same grid (120 nodes) the corresponding values are 13 and 1.14.

In order to illustrate the coordinate transformation "smoothness" the second derivative d^2f_2/dy^2 for the D & S flow is plotted in Fig.7b and its enlarged fragment in the vicinity of the step is shown in Fig.7c.

In Fig.8 an example is presented of a 142x120 grid used in the computations of the D & S flow. For this grid the maximum value of the turbulent coordinate $y^+=yv^*/\nu$ at the first near-wall node at the step side wall is not more than 1.6 and in the major part of the computational domain is varying in the range of 0.5-1.0.

3.3. Preliminary Numerical Studies

In order to make sure that the results obtained reflect the objective properties of the turbulence models being investigated, rather than numerical inaccuracies, some preliminary numerical studies were performed to eliminate the numerical errors associated with non-sufficiently fine grids and with uncertainties in the inflow/outflow boundary conditions.

Grid Refinement Study. A grid refinement study was carried out for all the turbulence models and test cases being considered. This study has shown that these models are relatively weakly sensitive to the grid-size. In particular, the comparison of the results obtained on the grids 40x40, 60x60, 90x90, 120x120, 120x180, and 180x120 on the basis of the ν_t-92, S-A, and M-SST models for both D & S and J & D flows permits to conclude that the solutions obtained on a 120x120 grid can be treated as virtually grid-independent ones. An additional substantiation of high quality of this grid is that it provides resolution of two secondary "corner vortices" being clearly seen in Fig.9 where a typical velocity field is depicted for the D & S flow with zero opposite-wall angle.

One specific computational property of the M-SST model was found out in the process of the grid refinement study. It turned out that the eddy viscosity profiles generated by this model in the region located downstream of reattachment had non-physical spikes (see Fig.10). To elucidate a mechanism responsible for these spikes formation special numerical experiments were carried out whose results are presented in Figs.11, 12.

In Fig.11 two functions, $a_1\omega$ and ΩF_2, are plotted, that define the eddy viscosity ν_t in the framework of the M-SST model in accordance with the relation

$$\nu_t = a_1 k / \max(a_1\omega,\ \Omega F_2) \tag{19}$$

One can see that switching from the first branch of ν_t to its second, "wake", branch occurs at y = 0.7H and reverse switching takes place at y = 1.5H. So the ν_t-spike is located in the wake region, and if one were to forbid the switching from one branch to another the ν_t profile should presumably become smooth. It is confirmed by Fig.12 where the profiles of ν_t computed with permitted and forbidden switching are depicted. Besides, if the switching is forbidden the profiles of ΩF_2 become virtually smooth as well. Since the function F_2 is smooth and close to unity in the region of the spikes, this fact means that the vorticity Ω profile is also practically smooth. Thus one can conclude that the spikes generated by the M-SST model in both ν_t and Ω profiles are caused by a nonlinear interaction between the eddy viscosity ν_t and the vorticity Ω when the former is determined through the latter in accordance with (19).

There is one more issue attention should be paid to when analyzing the nature of the spikes. They are located in the region of maximum grid clustering, where a slight non-smoothness of the grid transformation second derivative is observed (see Fig.7b). Thus the results obtained demonstrate for the M-SST model a lack of tolerance even of slight grid non-smoothness in the regions of its maximum clustering, if those regions are far from the wall.

As it was mentioned, along with the calculations on the basis of the S, S-A, and M-SST models, similar calculations were performed using the Chien low *Re* number *k*-ε *model [8]. It is well known now that due to the* so called non-locality of the models of such a type (associated with the dependence of the local flow properties on the corresponding wall friction value) they can not describe adequately the flow in the vicinity of separation and reattachment where the wall friction is close to zero. Our calculations of the backward-facing step flow on the basis of the Chien model have shown that this is completely true for this model as well: the use of its original version results in an unacceptably strong damping of the turbulence across the whole computational domain in the vicinity of the flow x-stations where the skin friction is equal to zero, namely near $x=0$ and $x=x_{reat}$. In order to cope with this issue we were forced to limit artificially the value of the friction coefficient C_f in the damping functions of the model, i.e., to replace the friction velocity $v^* = (\tau_w/\rho)^{1/2} = (\rho_0 U_0^2 (C_f/2)/\rho)^{1/2}$ by the following quantity:

$$\tilde{V}^* = \left(\rho_0 U_0^2 \left(\tilde{C}_f / 2\right) / \rho\right)^{1/2},$$

$$\text{with} \quad \tilde{C}_f = \max\left\{C_f, \varepsilon\right\}, \qquad (20)$$

where ε is some small constant. In our calculations we used $\varepsilon=10^{-4}$, but special experiments have shown that the results are virtually independent of the ε value at least in the range from $5\cdot10^{-5}$ to $2\cdot10^{-4}$.

Though this approach has no physical justification, it permits to get rid of the Chien model defect described above and to obtain quite reasonable results. Probably the same or quite similar tricks are used in all the simulations of the flows with separation and reattachment on the basis of the low Reynolds numbers *k*-ε models (see, for example [26]), but unfortunately not all the authors mention it. So all the calculations on the basis of the Chien model discussed bellow were actually obtained using its modification provided by (20).

As to the grid sensitivity of the Chien model it turns out that from the standpoint of the near wall value of the y^+ coordinate it needs approximately the same y-grid as all the other models considered in this work. However the values of the friction velocity predicted by the Chien model in the backward-facing step recirculation zone are significantly higher than those obtained on the basis of the other models (see below) which results in more severe demands on the grid. So for the Chien model a somewhat finer grid, 142x160, was used.

Finally, the grid refinement study for the M & B flow has shown that in this case virtually grid-independent solution can be obtained on a grid 170x140.

In order to estimate the effect produced by some uncertainty of the inflow boundary conditions and both, inflow and outflow, boundary positions some special simulations were performed with different inflow profiles *and with computational domains of different* size in the streamwise direction.

The results obtained show, in particular, that even the tangible discrepancy in the inlet eddy viscosity profiles generated by different turbulence models and by the DNS [27] does not affect noticeably the results of the simulation (see Fig.13).

As to the location of the inlet/outlet boundaries, it might be more important, especially for the evaluation of the pressure field as is clearly seen from Figs.14, 15. Therefore, one should keep in mind this vagueness in the inflow and outflow conditions while comparing the numerical and experimental data, especially for the M & B FFS flow, though our experiments have shown that varying the inlet/outlet positions in a certain reasonable range does not noticeably affect the flow quantities (other than the pressure).

3.4. Comparison of the results obtained using different turbulence models

Driver & Seegmiller Backward Facing Step Flow. In Fig.16 we compare the pressure field in the D & S flow, computed on the basis of the three turbulence models being examined. Attention should be paid to the fact that though the ν_t-92 and S-A models do not contain the so-called turbulent pressure term in the constitutive relation for the Reynolds stresses (it is impossible to account for this term straightforwardly in the framework of the ν_t-transport models) and the M-SST model does contain this term, the pressure fields generated by all three models are very close provided, of course, that the pressure p generated by the S-A and ν_t-92 models is compared with the full M-SST pressure $p+2/3\rho k$. Exactly the same results were obtained for all the other flows that have been studied in this work. So at least this restriction of the one-equation turbulence models does not play any significant role for the flows under consideration and, probably, for any other incompressible flows.

Figures 17-21 give an idea about the correspondence between the predictions obtained by the different models and the experimental data on the D & S flow.

As far as the velocity profiles are concerned, all the three models predict them quite satisfactorily (see Fig.17) though no model turns out to be able to describe accurately all the details of the velocity field. The M-SST model performs tangibly better in the recirculation zone while the ν_t-92 and S-A models are somewhat better in the region downstream reattachment. However the two latter models also underestimate the rate of the flow recovery, which is typical for all known turbulence models.

Exactly the same conclusion can be drawn with regard to the other flow quantities, for instance, for the shear-stress profiles depicted in Fig.18 and for the friction and pressure coefficient distributions presented in Figs.19, 20. To show more visually the capability of different models to predict the influence of the opposite wall angle α on the D & S flow characteristics, in Fig.21 the reattachment length and minimum value of the friction coefficient in the recirculation zone are plotted as functions of α.

An apparent conclusion from these figures is that the Chien k-ε model predicts skin friction significantly worse than any of the other three models we are dealing with, even though the results obtained on the basis of this model in our study are somewhat better than those published in the literature (it is probably due to finer grids used in the present work). This result is not very surprising, since the inability of the k-ε models to describe the flows with a strong adverse pressure gradient is commonly known now.

As to the ν_t-92, S-A, and M-SST models, from the standpoint of the wall angle dependence of the reattachment length, they are virtually equivalent, while the minimum friction is predicted somewhat better by the M-SST model for all the wall angle values.

The discrepancy between the results produced by different turbulence models is caused apparently by the difference in the eddy viscosity these models generate. The scale and character of this difference are clearly seen from Fig.22. The most significant difference is observed in the recirculation zone where the S-A model apparently overestimates the level of turbulence. In the region downstream the reattachment (x/H >6) the M-SST eddy viscosity is somewhat lower than those given by S-A and ν_t-92. As to the Chien model, just as one could expect, it generates too high an eddy viscosity in both separation and flow recovery zones.

Jovic & Driver Backward-Facing Step Flow. Fig.23 shows the eddy viscosity profiles, generated by the different models for the J & D flow with the Reynolds number 5000, and Figs.24, 25 illustrate the correspondence between the predicted and experimental profiles of the mean velocity and shear-stresses. Finally, in Fig.26 the longitudinal friction and pressure coefficient distributions are presented for the J & D flow with Reynolds number 5000.

The main conclusion from Figs.23-26 is that all the three models being studied react adequately to the Reynolds number drop and, in particular, are able to predict the sharp increase of the maximum value of the friction coefficient in the recirculation zone that was observed in the experiments [6]. This trend is seen more clearly from Fig.27 where the numerical and experimental data on the minimum C_f are plotted as a function of the Reynolds number. Again, it is difficult to give a preference to any of ν_t-92, S-A or M-SST models but their superiority over the Chien model, especially at high *Re* numbers, is undoubtful.

Moss & Baker Forward-Facing Step Flow. In Fig.28 a comparison is presented of the general views of the flow pattern in the vicinity of the step observed in the experiment and predicted by the ν_t-92, S-A, and M-SST turbulence models. When analyzing these results one should take into account that the experimental stream function contours were obtained not directly (by the flow visualization) but by integrating the measured velocity field, and so can not claim to be very accurate especially near reattachment. Nevertheless, it can be concluded that for this flow the S-A model gives somewhat better results than the two others: the M-SST model apparently underestimates the length of the second separation zone, while the ν_t-92 model, on the contrary, predicts flow reattachment too far.

Fig.29 gives a more detailed idea about the quality of the velocity field prediction provided by different models.

Upstream of the first recirculation zone ($x/H < -1$) all the three models give virtually the same *u*-velocity profiles being in good correspondence with the experimental data.

In the vicinity of the step the discrepancy between the results obtained by the different models still remains virtually negligible, but exactly in this region, that is in the region of the strong flow acceleration, the most significant disagreement between the numerical and experimental data is observed.

Downstream of the step the difference between the models gets more tangible. Just as in the case of the backward-facing step flow it is difficult to give a definite preference to any of the models here since no model can equally accurately capture the details of the velocity field in the all experimental sections downstream the step. However it can be concluded that "in average" the S-A model has some advantage over the two others in this part of the flow.

The fact that the models react quite differently to the fast variation of the flow characteristics right upstream and downstream the step is clearly seen from Fig.30 where the eddy viscosity profiles are presented. In particular, the ν_t-92 and S-A eddy viscosities upstream the step start to change abruptly (to react to the step) a great deal later than the M-SST eddy viscosity. As a result of this "delay" the maximum value of the M-SST eddy viscosity at $x = 0$ is approximately three times as high as the corresponding ν_t-92 and S-A values.

As to the pressure coefficient prediction, all the three models give almost the same results being close to the experiment except for the close vicinity of the step (Fig.31).

Unfortunately the paper by Moss & Baker does not contain any data on the experimental shear stress profiles and wall friction distribution. Due to that lack of the data it is difficult to say for now which model from the three being examined performs better as applied to the forward-facing step flow. However, just as for the backward-facing step flow, all the three models turn out to be much more realistic than the k-ε model. As a substantiation, in Figs.31, 32 a comparison is presented of the results obtained in the present work with those obtained for the same flow by Park & Chung [28] on the basis of a special modification of the k-ε model taking into account the streamline curvature.

3.5. Computational efficiency of different turbulence models

One of the objectives of the present study was to compare the computational efficiency of the ν_t-92, S-A, and M-SST models as applied to the flows we considered, in the framework of the same numerical algorithm. Fig.33,a-c, show the typical convergence histories of the flow solver for the J & D flowfield obtained on the grid 60x120 with all the three models. For all the cases the same value of the Courant number, $CFL = 4.0$, was used coupled with a space-varying time-stepping strategy permitting to accelerate the convergence on nonuniform grids. The solutions are considered converged when the maximum nondimensional residual has become less than $5 \cdot 10^{-6}$, which corresponds to a drop of the residual for all the variables by over 4 orders of magnitude. For the S-A model this criterion was satisfied in 540, for the ν_t-92 model in 660, and for the M-SST model in 1360 iterations. Thus from the standpoint of the convergence rate, in the framework of the approximate factorization technique being used in the present work, the S-A model turned out to be the fastest and the M-SST model the slowest one. Since the former is a one-equation model and the latter is a two-equation one, the difference of the CPU time for these models is somewhat (≈10%) higher than that in the number of iterations.

One specific effect should be mentioned concerning the convergence rate of the ν_t-92 model. It was found out that it degraded significantly when relatively coarse y-grids were used. This effect is demonstrated by Fig.33,d where the convergence history for the ν_t-92 model is depicted for the J & D (Case 1) flow for the grid with 60 nodes in the *y* direction. One can see that it suffers from long-period oscillations of the maximum residual values. The analysis of the results shows that the oscillations are caused by the ν_t-residual jumps in the first near-wall node at some *x*-coordinate downstream of reattachment. In the process of convergence to a steady-state the "jump" node moves downstream, the period of the oscillations being associated exactly with changing of its *x*-coordinate. Once the oscillations stop (it occurs when the *x*-coordinate of the "jump" reaches the outlet boundary of the computational domain), the residuals start dropping monotonically with the rate typical for a finer grid.

Though the mechanism of these oscillations is not quite clear for now, some elucidation can be found in Fig.34 where a comparison is presented of the results obtained on the basis of the ν_t-92 model for a flat plate boundary layer on the different *y*-grids. If the grid is not fine enough the solution has a sharp jump moving upstream with grid refinement. At the same time the turbulent coordinate of the first near wall node in the section of the boundary layer, where the jumps take place, keeps an approximately constant value, $y^+ = 3.2$. The analysis of the separate terms of the ν_t-92 transport equation shows that in the vicinity of the jumps the budget of the source and dissipative terms at the edge of the viscous sublayer experiences a crucial changing resulting in the fast rebuilding of the near-wall part of the velocity profiles and skin friction jumps observed here.

Thus it can be supposed that the long-period oscillations in the Navier-Stokes convergence to a steady-state shown in Fig.33,d might be caused by a similar effect, i.e., by periodical changing of the flow structure due to changing of the near-wall y^+ values in the process of convergence.

Concluding Remarks

A comparative study is performed of three recently developed turbulence models, two being one equation, ν_t-models, and one the two equation, k-ω model, as applied to the backward- and forward-facing step flows. It turns out that though no model does capture all the details of the flows under consideration both in the recirculation zones and in the region of the flow recovery, all the three models perform significantly better than the conventional k-ε model and its modifications, even those ones developed exactly for the flows under consideration. In particular, they provide for much better prediction of the reattachment length and skin friction in a wide range of opposite wall angles and Reynolds number.

It is difficult to give the definite preference to any of three examined models for all the flow quantities in all the cases considered. However it looks like for the backward-facing step the Menter SST model performs tangibly better than two others inside the recirculation region, while the ν_t-92 seems to be somewhat more realistic in the region downstream reattachment. On the contrary, as applied to the forward-facing step flow the Spalart-Allmaras model "in average" performs noticeably better than the ν_t-92 and somewhat Menter SST ones.

From the computational standpoint the Spalart-Allmaras model is the most efficient and the Menter SST model is the most slow converging and time consuming, at least in the framework of the approximate factorization technique being used in the present work. Besides, the Menter SST model turns out non-tolerant of even slight non-smoothness of grid in the region of its maximum clustering, and convergence rate of the ν_t-92 model drops significantly when relatively coarse grids are used.

Acknowledgements

This study was carried out under the agreement with the Boeing Operations International Inc. with the technical assistance of the Boeing Technical Research Center in Moscow. It was also supported by the Russian Basic Research Foundation (grants numbers *93-013-17687 and 94-02-06365). The authors* would like also to thank Dr. Philippe Spalart from the Boeing Commercial Airplane Group for numerous fruitful discussions of the general problems of turbulence modeling and of the results of the present work, in particular, and Drs. V. Kuznetsov, A. Lebedev, and V. Sklyarov for their valuable impact in development of the ν_t-92 model.

REFERENCES

1. Gulyaev A.N., Kozlov V.Ye., Secundov A.N., "A Universal One-Equation Model for Turbulent Viscosity", *Fluid Dynamics*, Vol.28, No.4, pp.485-494, 1993 (Translated from Russian, Consultants bureau, New York)

2. Spalart P.R., Allmaras S.R., "A One-Equation Turbulence Model for Aerodynamic Flows", AIAA Paper 92-0439, 1992.

3. Menter, F.R., "Zonal Two Equation k-ω Turbulence Models for Aerodynamic Flows", AIAA Paper 93-2906, 1993.

4. Driver, D.M. and Seegmiller, H.L., "Features of a Reattachment Turbulent Shear Layer in Divergent Channel Flow", *AIAA Journal*, Vol.23, No.2, 1985.

5. Jovic, S, and Driver D.M., "Backward-Facing Step Measurement at Low Reynolds Number, Re = 5000", NASA TM 108807, 1994.

6. Jovic, S. and Driver D.M., "Reynolds Number Effect on the Skin Friction in Separated Flows Behind a Backward-Facing Step", Technical Note (Sent to Exp.of Fluid), 1993.

7. Moss, W.D., Baker, S., "Re-Circulating Flows Associated with Two-Dimensional Steps", *Aeronautical Quarterly*, Pt.3, Aug.1980, pp.151-172.

8. Chien, J.Y., "Prediction of Channel Boundary Layer Flows with a Low-Reynolds-Number Turbulence Model", *AIAA Journal*, Vol.20, No.1, pp. 332-338, 1982.

9. Bradshaw P., Launder B., Lumley J., "Collaborative Testing of Turbulence Models", AIAA Paper 91-0215, 1991.

10. Kovasznay L.S.G., "Structure of the Turbulent Boundary Layer", *Physics of Fluids*, Vol.10, No.9, pt.2, 1967, pp.25-30.

11. Nee V.W., Kovasznay L.S.G., "Simple Phenomenological Theory of Turbulent Shear Flows", *Physics of Fluids*, vol.12, No.3, 1969, pp.473-484.

12. Wilcox, D.C., "Reassessment of the Scale-Determining Equation for Advanced Turbulence Models", *AIAA Journal*, Vol.26, No.11, 1988, pp.1299-1310.

13. Rogers, S.E., Menter, F.R., Durbin, P.A., Mansour, N.N., "A Comparison of Turbulence Models in Computing Multi-Element Airfoil Flows", AIAA Paper, 94-0291, 1994.

14. Secundov, A.N., "Application of a Differential Equation for Turbulent Viscosity to the Analysis of Plane Non-self-similar Flows", *Fluid Dynamics*, Vol.6, No.5, 1971, pp.828-840 (Translated from Russian, Consultants bureau, New York).

15. Abramovich, G.N., Krasheninnikov, S.Yu., and Secundov, A.N., "Turbulent Flows in the Presence of Body Forces and Non-Self-Similarity", Mashinostroenie, Moscow, 1975, 93 pp. (in Russian).

16. Lebedev A.B., Secundov A.N., "Use of the Equation for Turbulent Viscosity to Describe the Flow Near a Rough Surface", *Fluid Dynamics*, Vol.10, No.5, *1975*, pp.741-744 (Translated from Russian, Consultants bureau, New York).

17. Kozlov V.E, Secundov A.N., Smirnova I.P., "Models of Turbulence for the Description of a Flow in a Jet of Compressible Gas", *Fluid Dynamics*, Vol.21, No.6, 1986, pp.875-881. (Translated from Russian, Consultants bureau, New York).

18. Spalart P.R., Allmaras S.R., "A One-Equation Turbulence Model for Aerodynamic

Flows", *La Recherche Aerospatiale*, 1994, No.1, pp.5-21.

19. Batchelor G. K., Gill A. E., "Analysis of the stability of axisymmetric jets", *J.Fluid Mech.*, 1962, Vol.14, pp.529-551.

20. Secundov A.N., "Turbulence in a Supersonic Flow and Its Interaction with a Shock Wave". *Fluid Dynamics*, Vol.9, No.2, 1974, pp.166-172. (Translated from Russian, Consultants bureau, New York)

21. Kuznetsov V.R., Lebedev A.B., Secundov A.N., Smirnova I.P., "Calculation of a Turbulent Diffusion Combustion Flame Taking Account of Concentration Pulsations and Archimedian Forces", *Fluid Dynamics*, 1977, No.1, pp.24-33 (Translated from Russian, Consultants bureau, New York)

22. Lele S.K., "Compressibility Effects on Turbulence", *Annu.Rev.Fluid Mech.*, 1994, Vol.26, pp.211-254.

23. Le, H., Moin, P., and Kim, J., "Direct Numerical Simulation of Turbulent Flow over a Backward-Facing Step", The Ninth Symposium on Turbulent Shear Flows, Kyoto, Japan, Aug.16-18, 1993, pp.13-2-1 - 13-2-5.

24. Strelets, M.Kh., and Shur, M.L., "Method of Scaling the Compressibility in Calculating Stationary Flows of Viscous Gas at Arbitrary Mach Numbers", *U.S.S.R. Computational Mathematics and Mathematical Physics*, Vol.28, No.1, pp.165-173, 1988 (Translated from Russian, Consultants bureau, New York).

25. Shur, M.L., "Compressibility Scaling Method for Arbitrary Mach Number Navier-Stokes Simulation of Internal Reactive Gas Mixture Flow", The Seventh Int.Conf. on Numerical Methods in Laminar and Turbulent Flow, Stanford, July 15-19, 1991, Vol.7, Pt.2, pp.1526-1536.

26. Martelli, F., and Michelassi, V., "An Implicit Factored Solver for Inner Turbulent Flows", AIAA Paper 88-3099, 1988.

27. Spalart, P.R., "Direct Simulation of a Turbulent Boundary Layer up to Re_θ=1410", *J.Fluid Mech.*, Vol.187, 1988, pp.61-98.

28. Park, S.W., and Chung, M.K., "Curvature-Dependent Two-Equation Model for Prediction of Turbulent Recirculating Flows", *AIAA Journal*, Vol.27, No.3, pp.340-344, 1989.

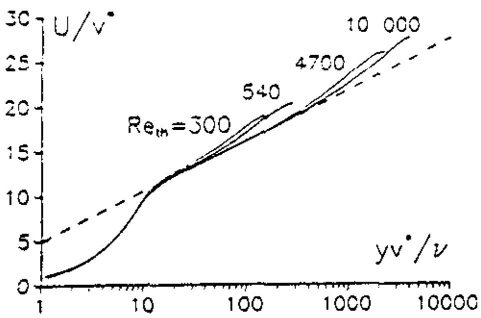

Figure 1. Velocity profiles for a flat plate boundary layer

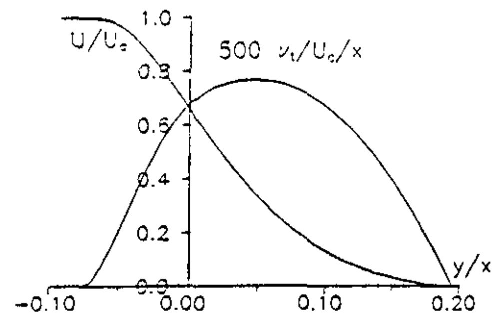

Figure 2. Velocity and eddy viscosity profiles for a mixing layer

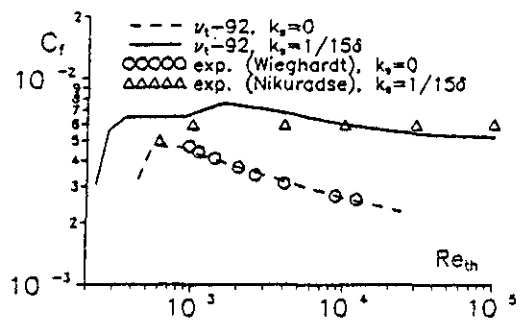

Figure 3. Skin friction distribution on a smooth and rough surface

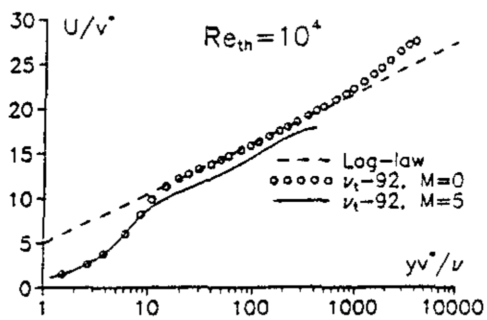

Figure 4. Mach number effect on velocity profiles for a flat plate boundary layer

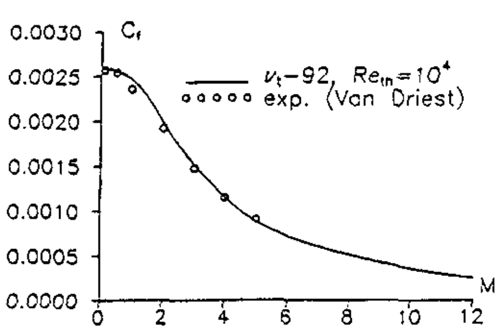

Figure 5. Mach number effect on the skin friction coefficient

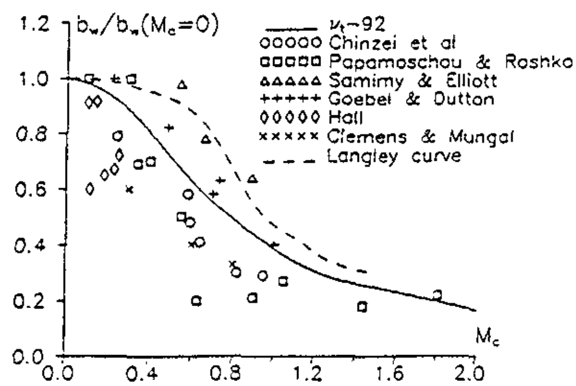

Figure 6. Mach number effect on a mixing layer thickness $b_w = (U_{max} - U_{min})/(\partial U/\partial y)_{max}$

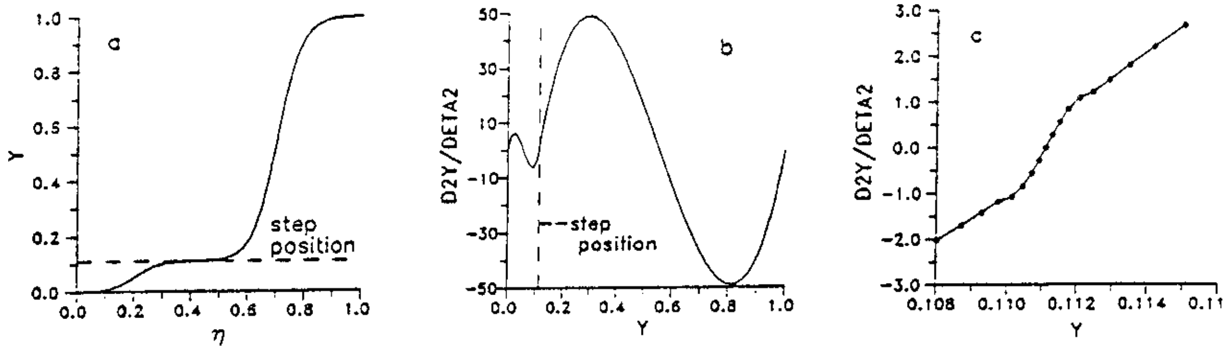

Figure 7. Y-coordinate transformation for the D&S flow.
(a): $y(\eta)$; (b): $d^2y/d\eta^2$; (c): enlarged fragment of Fig.7-b in the vicinity of step

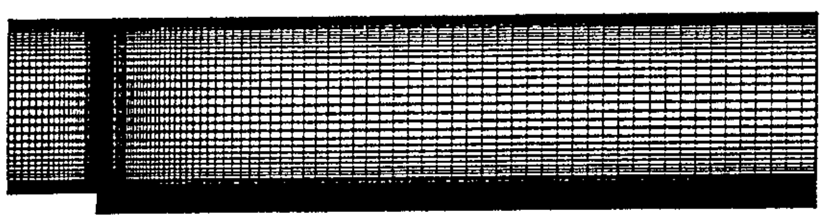

Figure 8.An example of grid used for the D&S flow

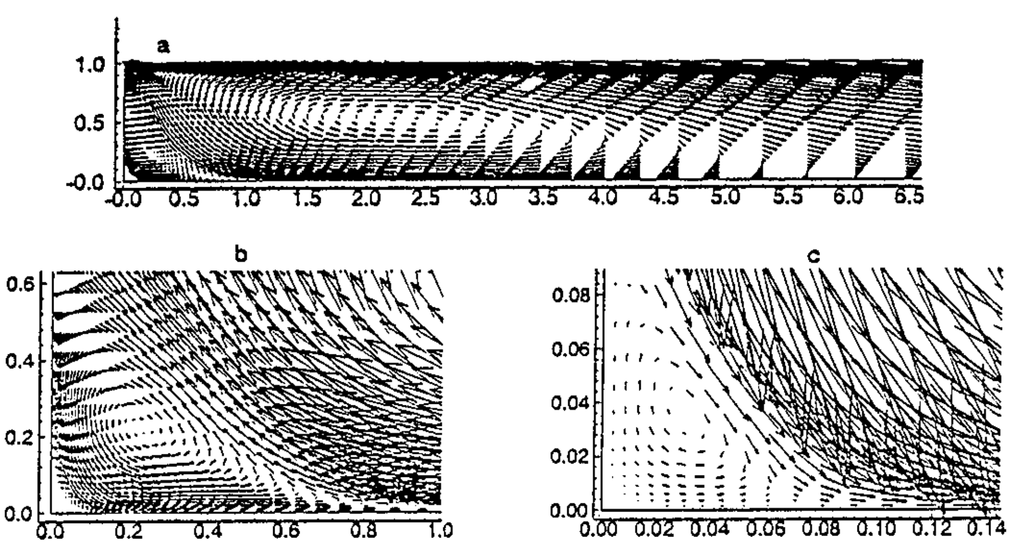

Figure 9. Velocity vector field for the D&S flow with zero opposite wall angle.
(a): fragment of the flow in the vicinity of step; (b): enlarged fragment of Fig.9-a;
(c): enlarged fragment of Fig.9-b

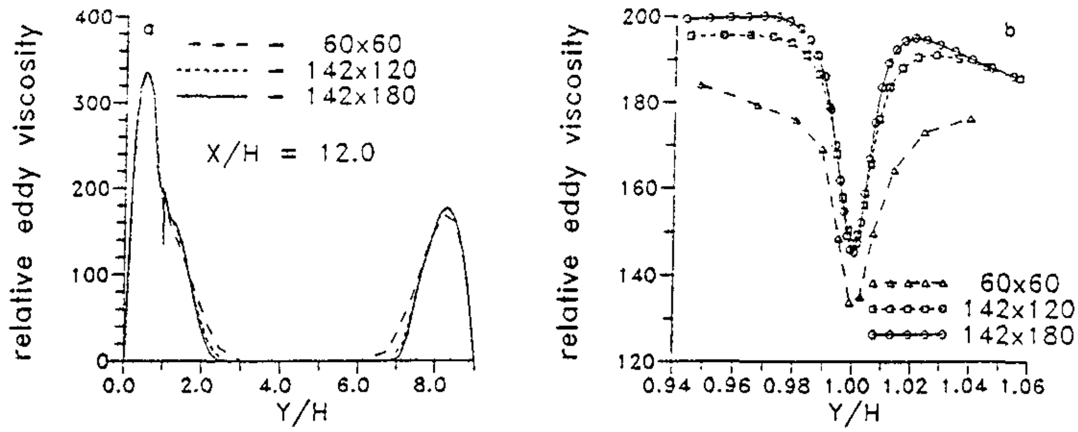

Figure 10. M-SST eddy viscosity profiles on different grids for the D&S ($\alpha=0^{\circ}$) flow. (a): x/H=12; (b): enlarged fragment of Fig.10-a in the vicinity of y/H=1

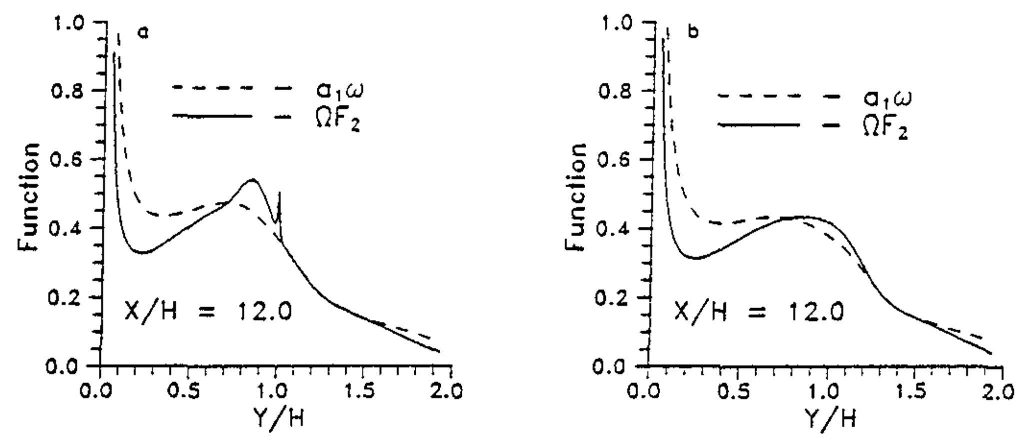

Figure 11. Functions $a_1\omega$ and ΩF_2, used for the calculation of eddy viscosity in the M-SST model: $\nu_t = a_1k/\max(a_1\omega, \Omega F_2)$. (a): with switching to ΩF_2 branch; (b): without switching

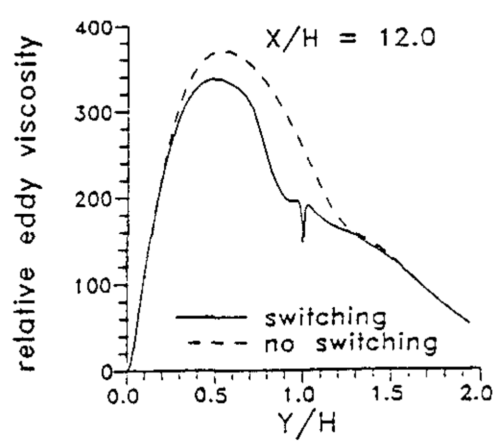

Figure 12. M-SST eddy viscosity profiles with and without switching from $a_1\omega$ to ΩF_2 branch

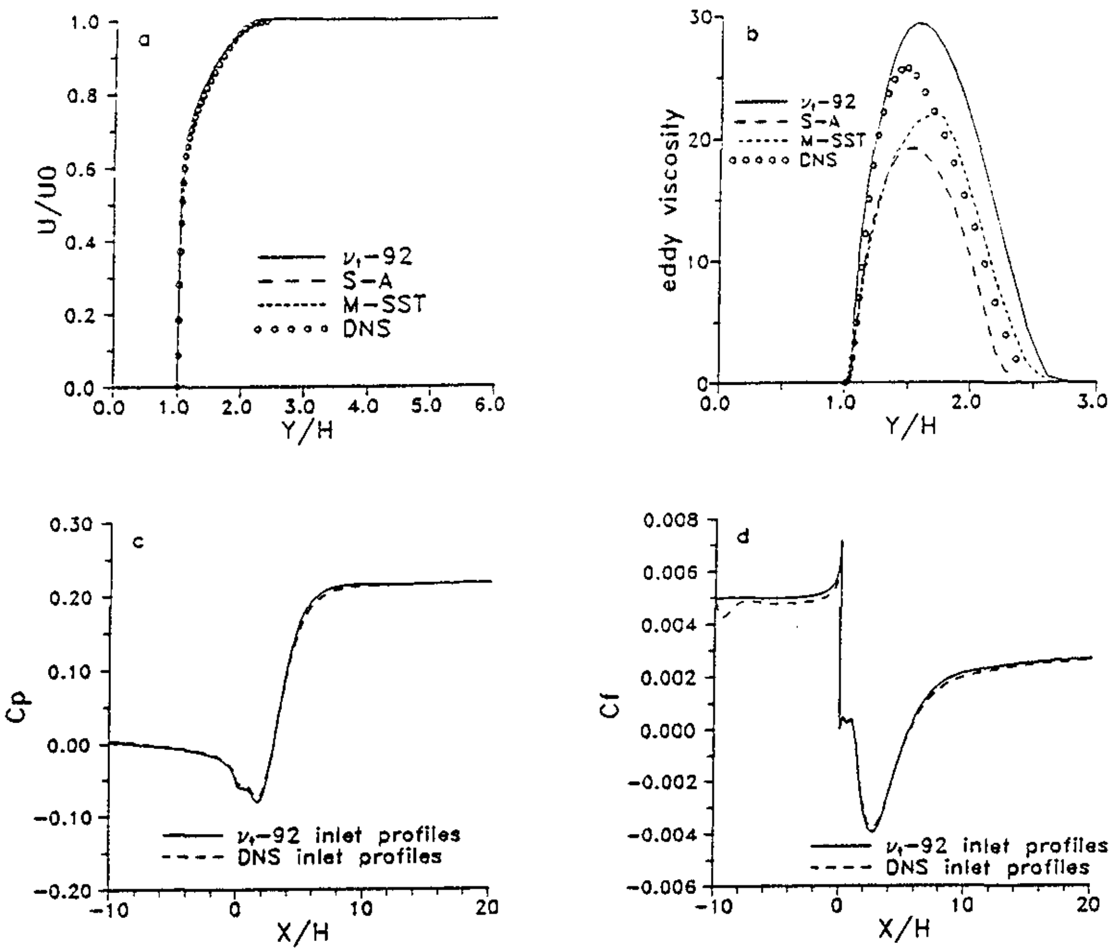

Figure 13. Effect of inlet profiles on the J&D (case 1) flowfield. (a),(b): inlet u- and v_t-profiles generated by the three models and by the DNS [27]; (c),(d): c_f and c_p coefficients obtained on the basis of the v_t-92 model with inlet profiles generated by the v_t-92 and by the DNS

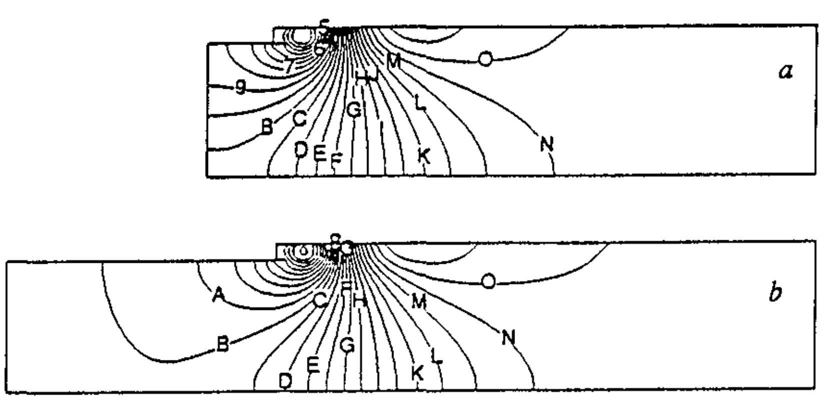

Figure 14. Effect of the inflow boundary location on the D&S (α=0°) flowfield.
(a),(b): pressure field (a: x_{inlet}=-4H, b: x_{inlet}=-16H);

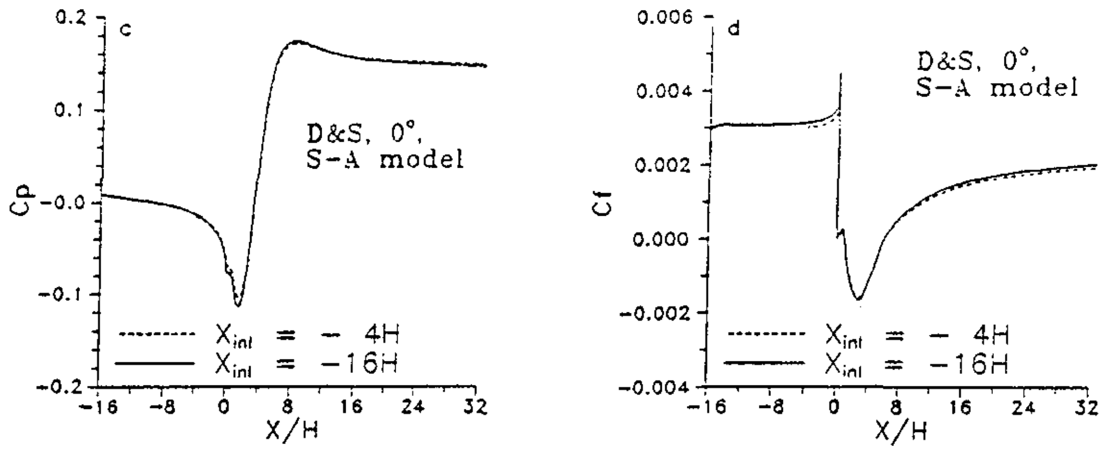

Figure 14 (continued). (c),(d): pressure and skin friction distributions for the step-side wall

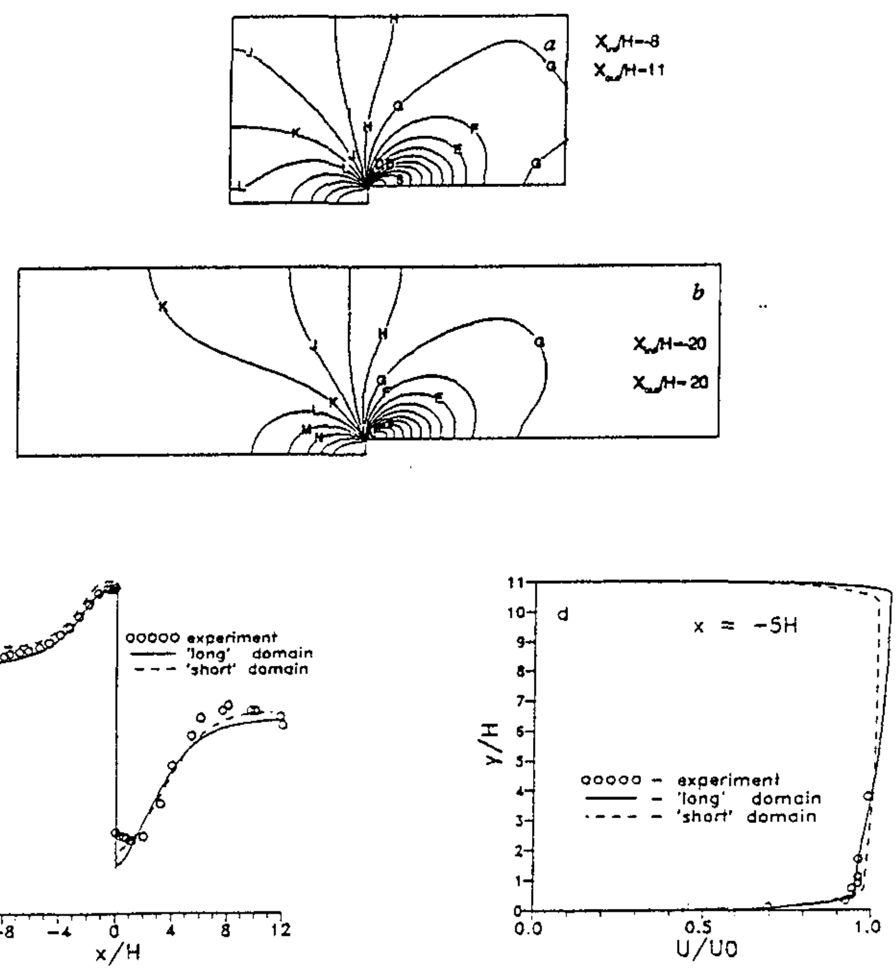

Figure 15. Effect of inflow and outflow boundaries location on the pressure field (a,b), c_p distribution along the step-side wall (c), and velocity profile upstream the step (d) for the M&B forward-facing step flowfield (computations on the basis of the ν_t-92 model).

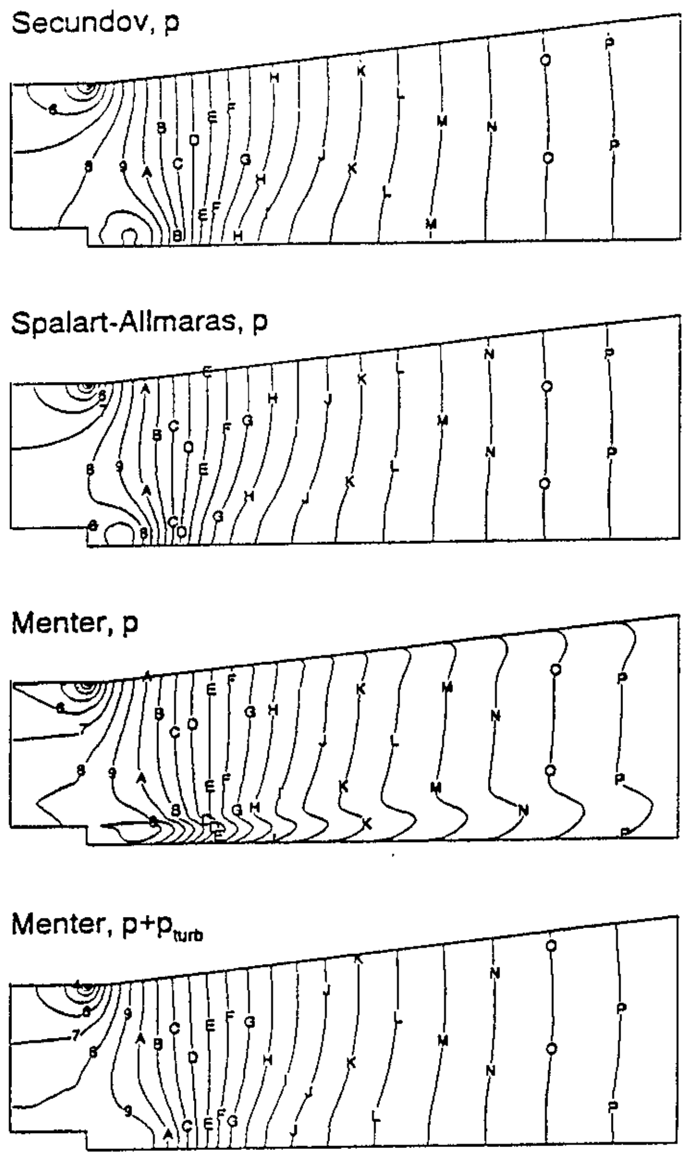

Figure 16. Comparison of pressure fields for the D&S (α=6°) flow obtained on the basis of the three turbulence models

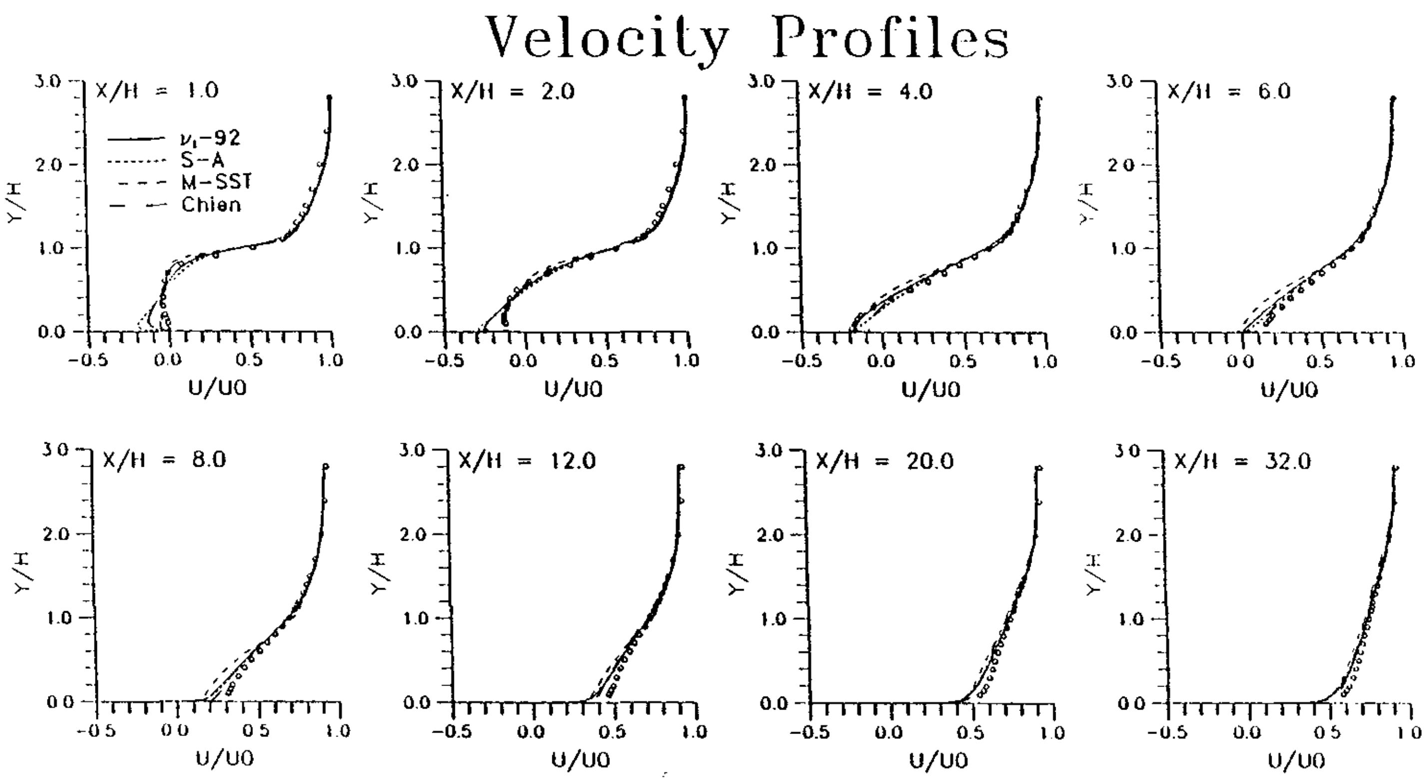

Figure 17. Velocity profiles for the D&S (α=0°) flow

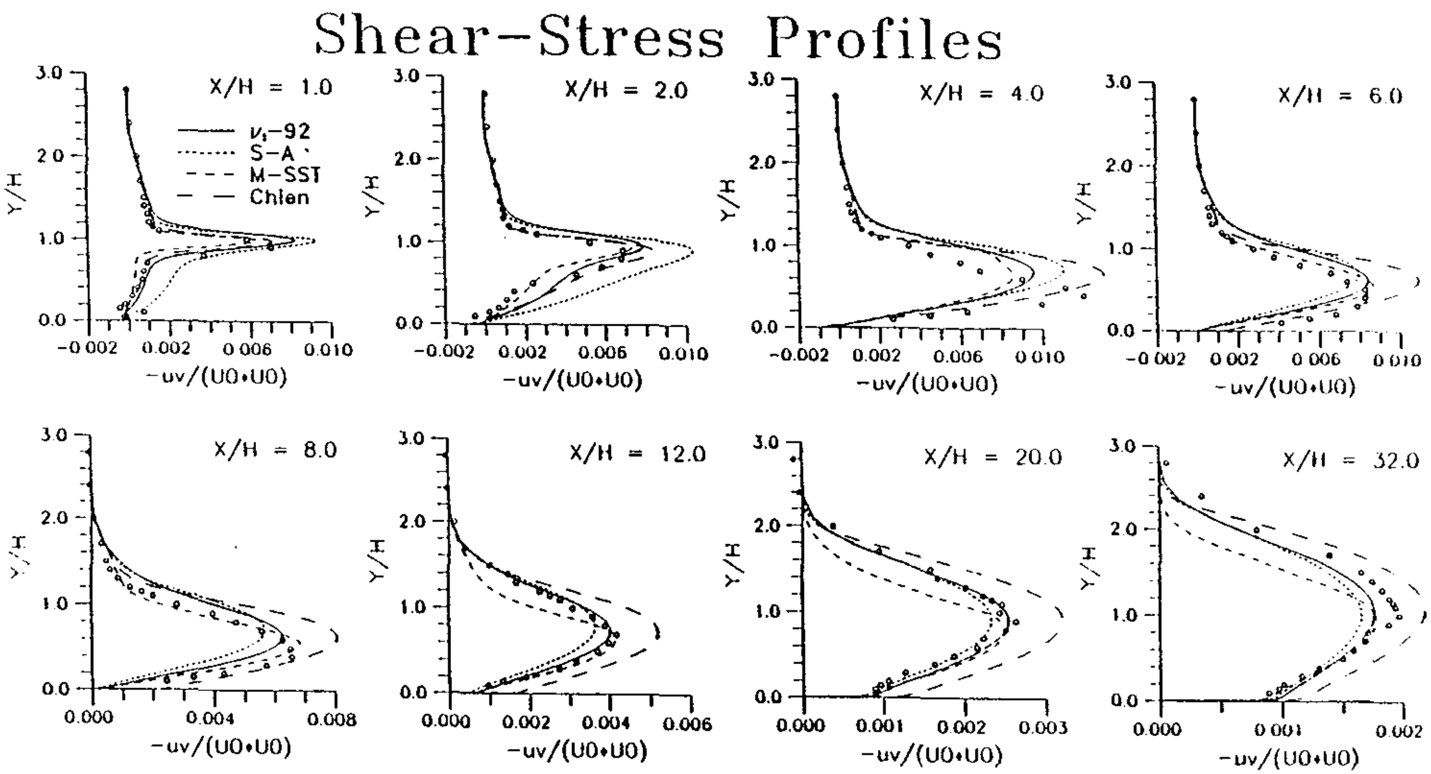

Figure 18. Shear stress profiles for the D&S (α=0°) flow

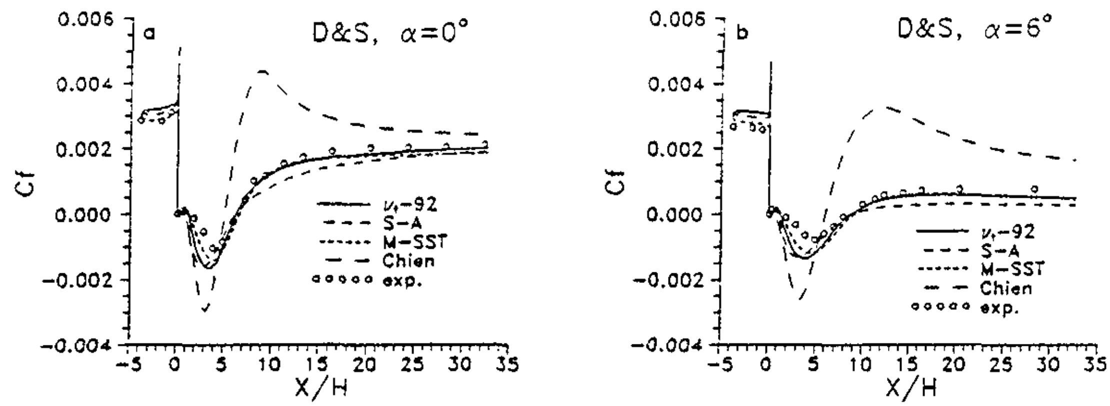

Figure 19. Skin friction distribution along the step-side wall for the D&S, α=0° and α= 6°, flow

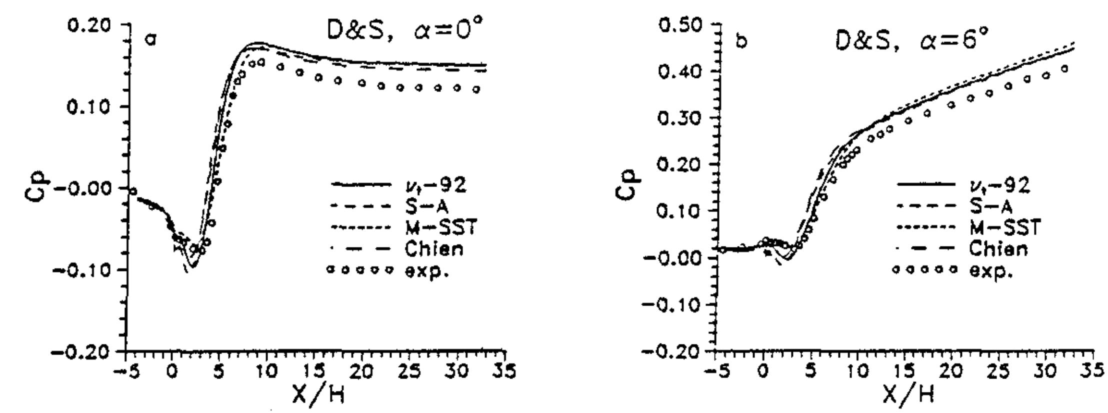

Figure 20. Pressure coefficient distribution along the step-side wall for the D&S, α=0° and α=6°, flow

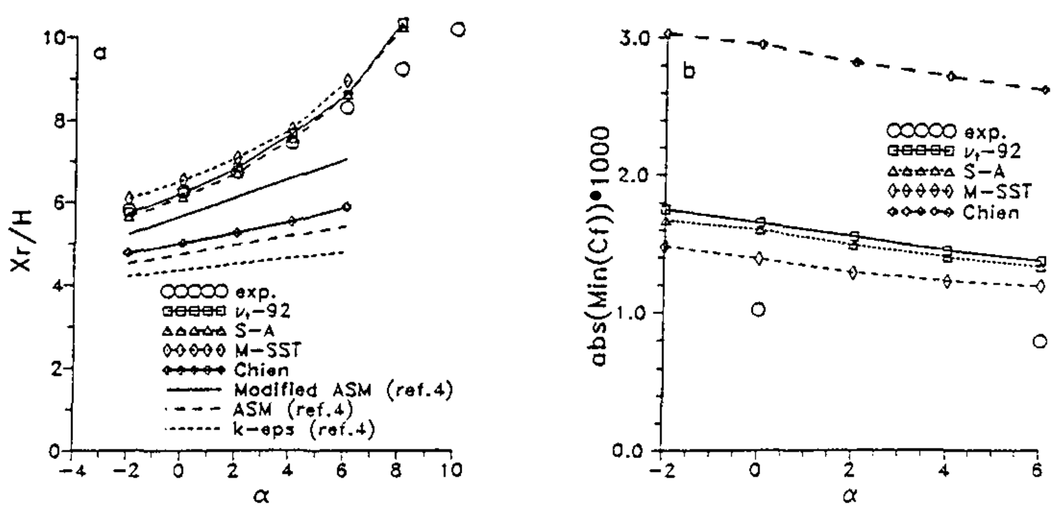

Figure 21. Effect of the opposite wall angle on the reattachement length (a) and minimum c_f value in the recirculation zone (b) for the D&S flow

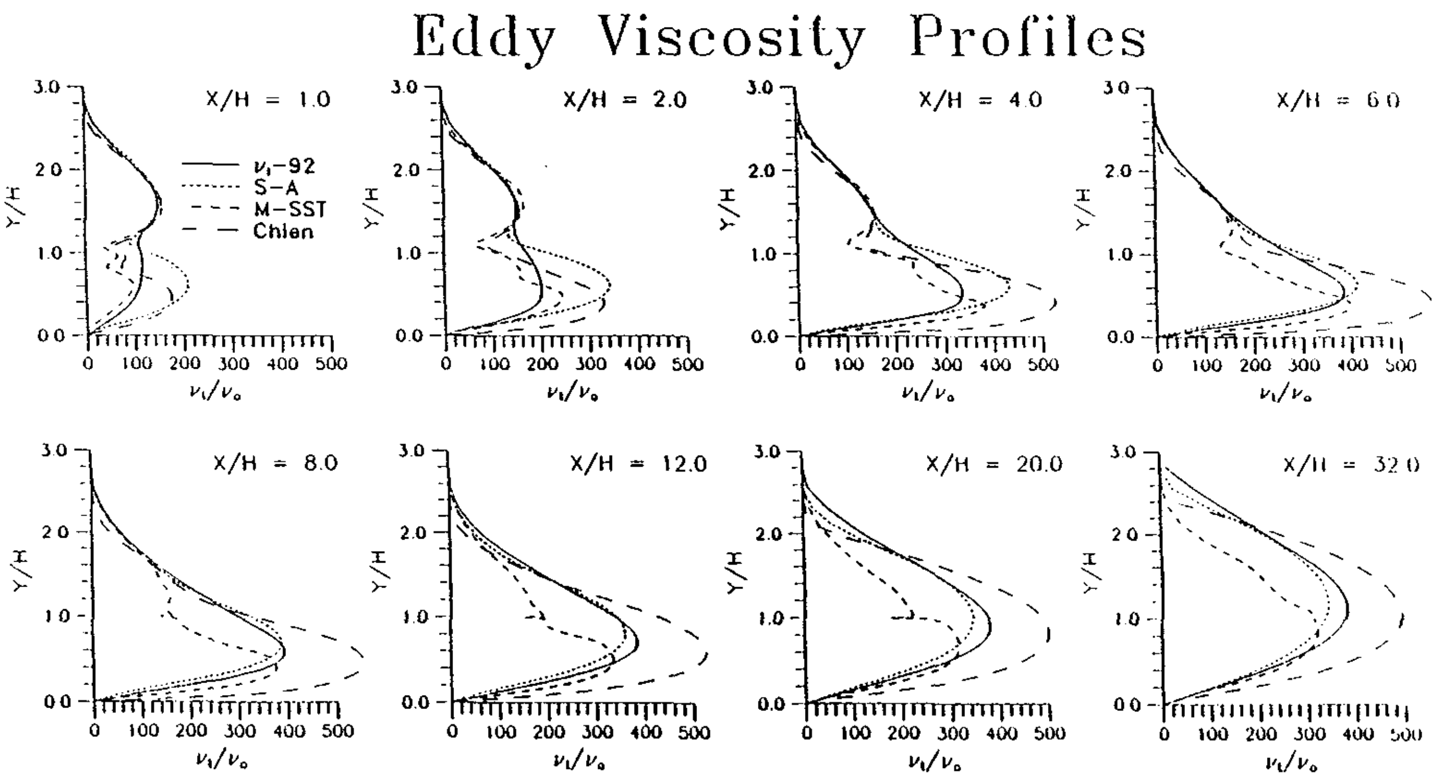

Figure 22. Eddy viscosity profiles for the D&S (α=0°) flow

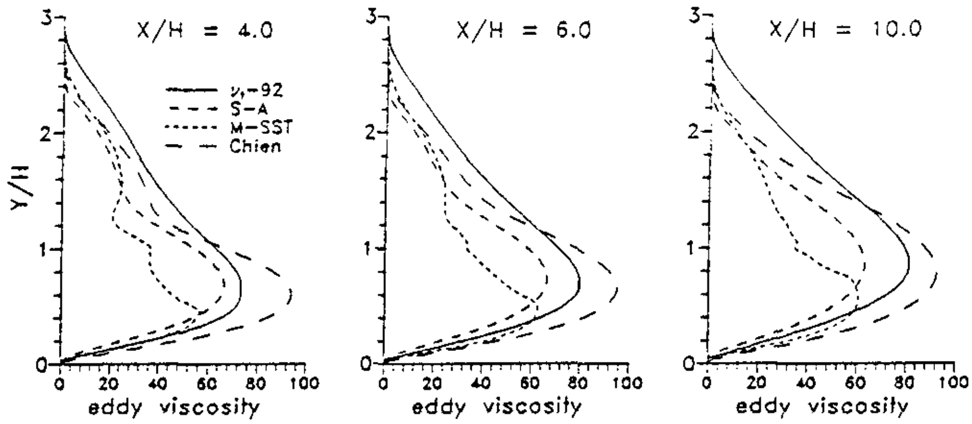

Figure 23. Eddy viscosity profiles for the J&D, case 1, flow

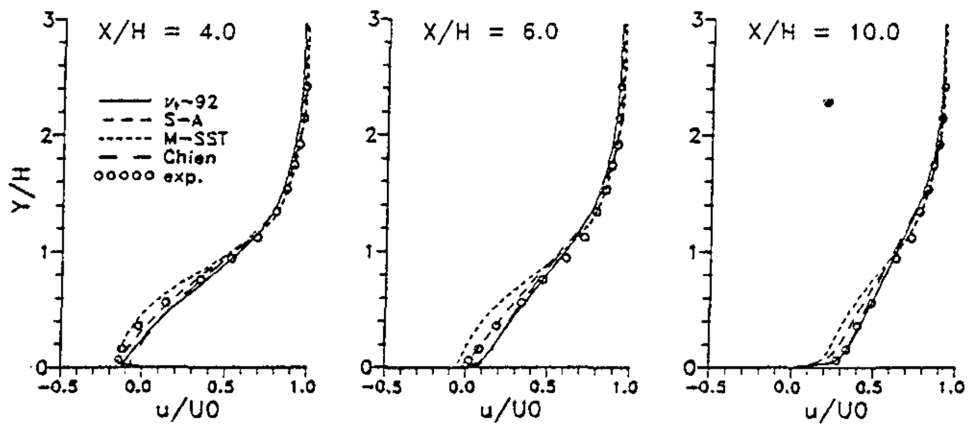

Figure 24. Velocity profiles for the J&D, case 1, flow

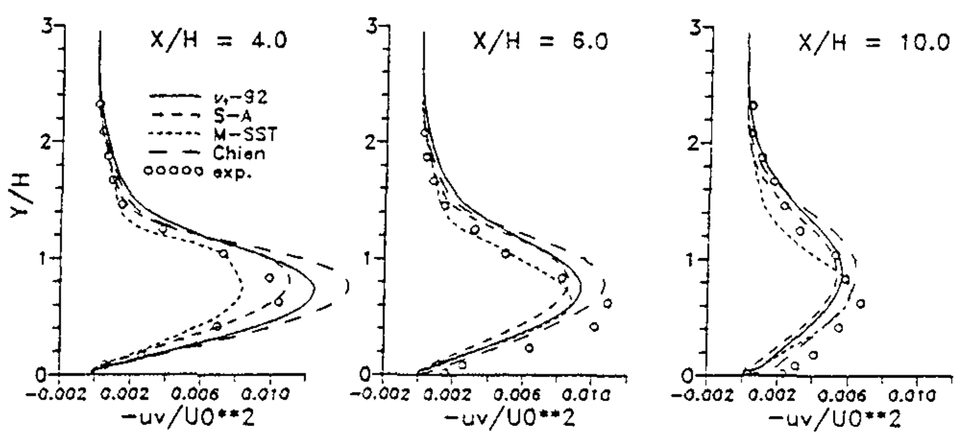

Figure 25. Shear stress profiles for the J&D, case 1, flow

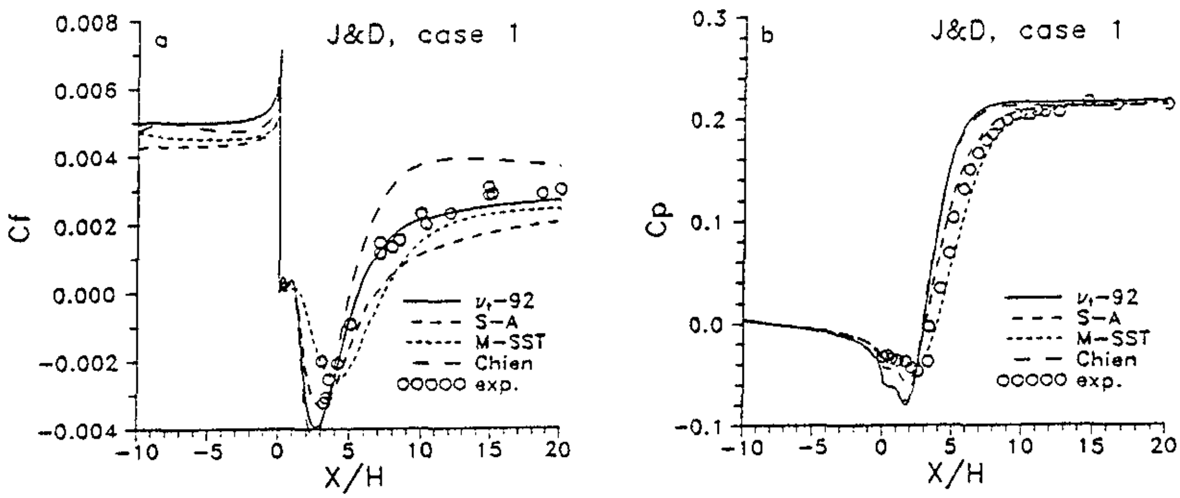

Figure 26. Skin friction and wall pressure distribution for the J&D, case 1, flow

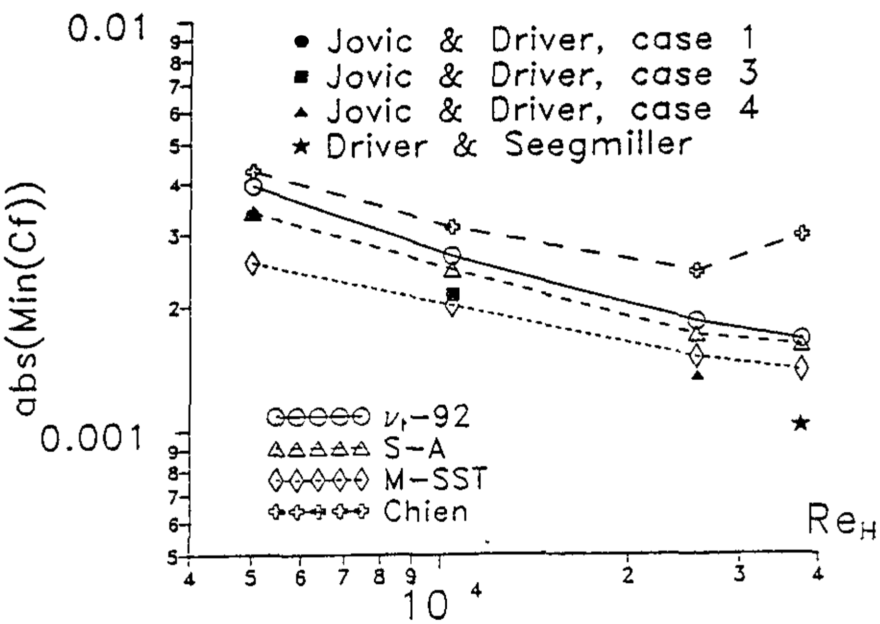

Figure 27. Effect of Reynolds number Re_H on minimum skin friction value in the recirculation zone

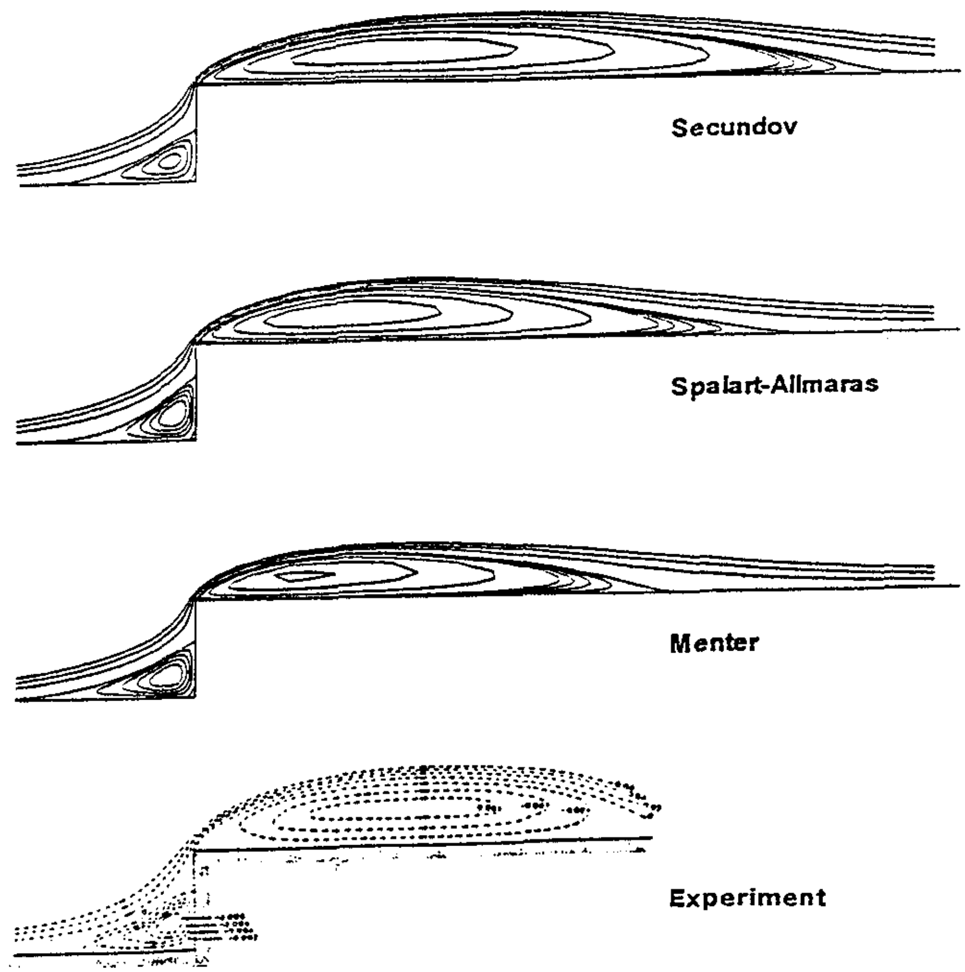

Figure 28. General view of the flow pattern predicted by the different models for the M&B forward-facing step flow

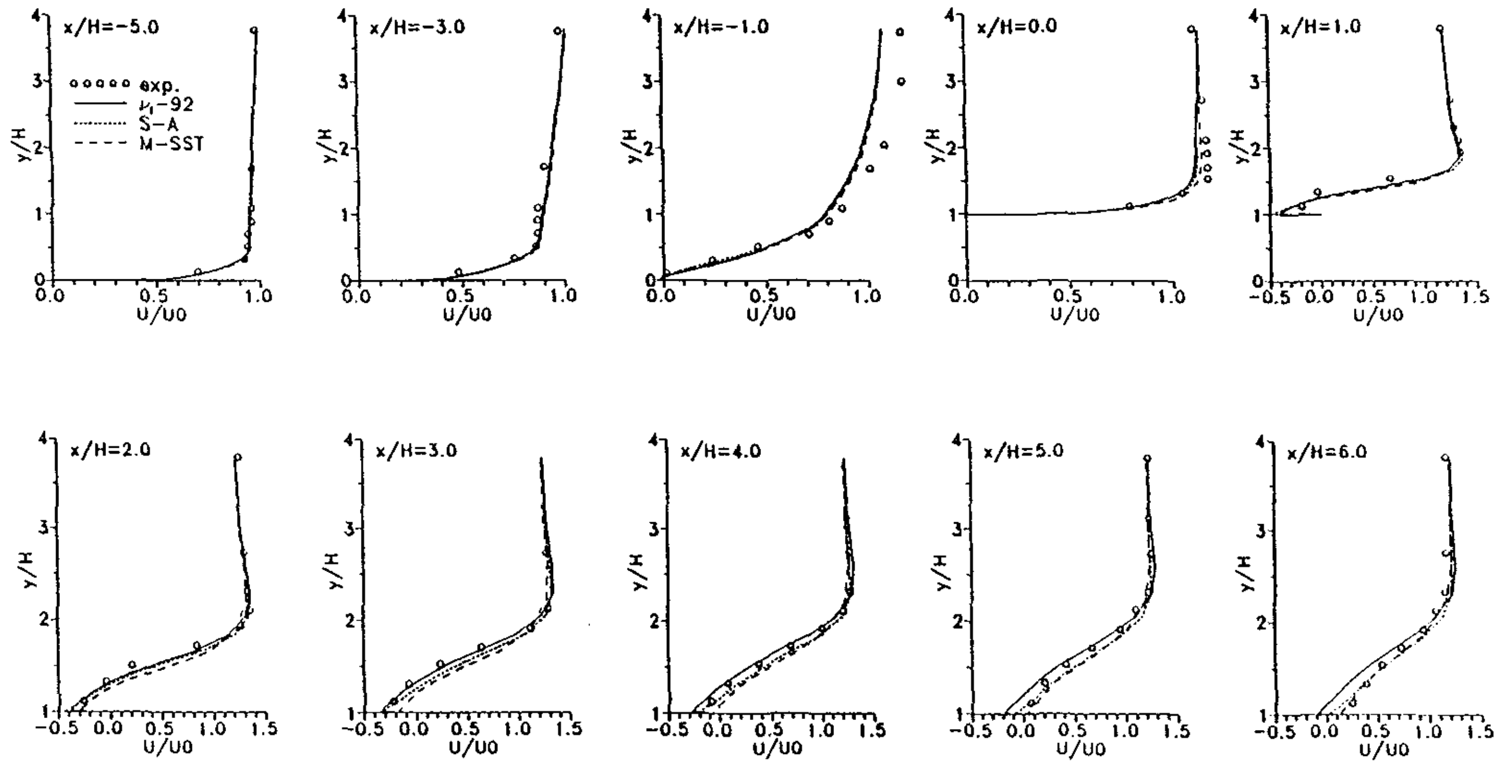

Figure 29. Velocity profiles for the M&B forward-facing step flow

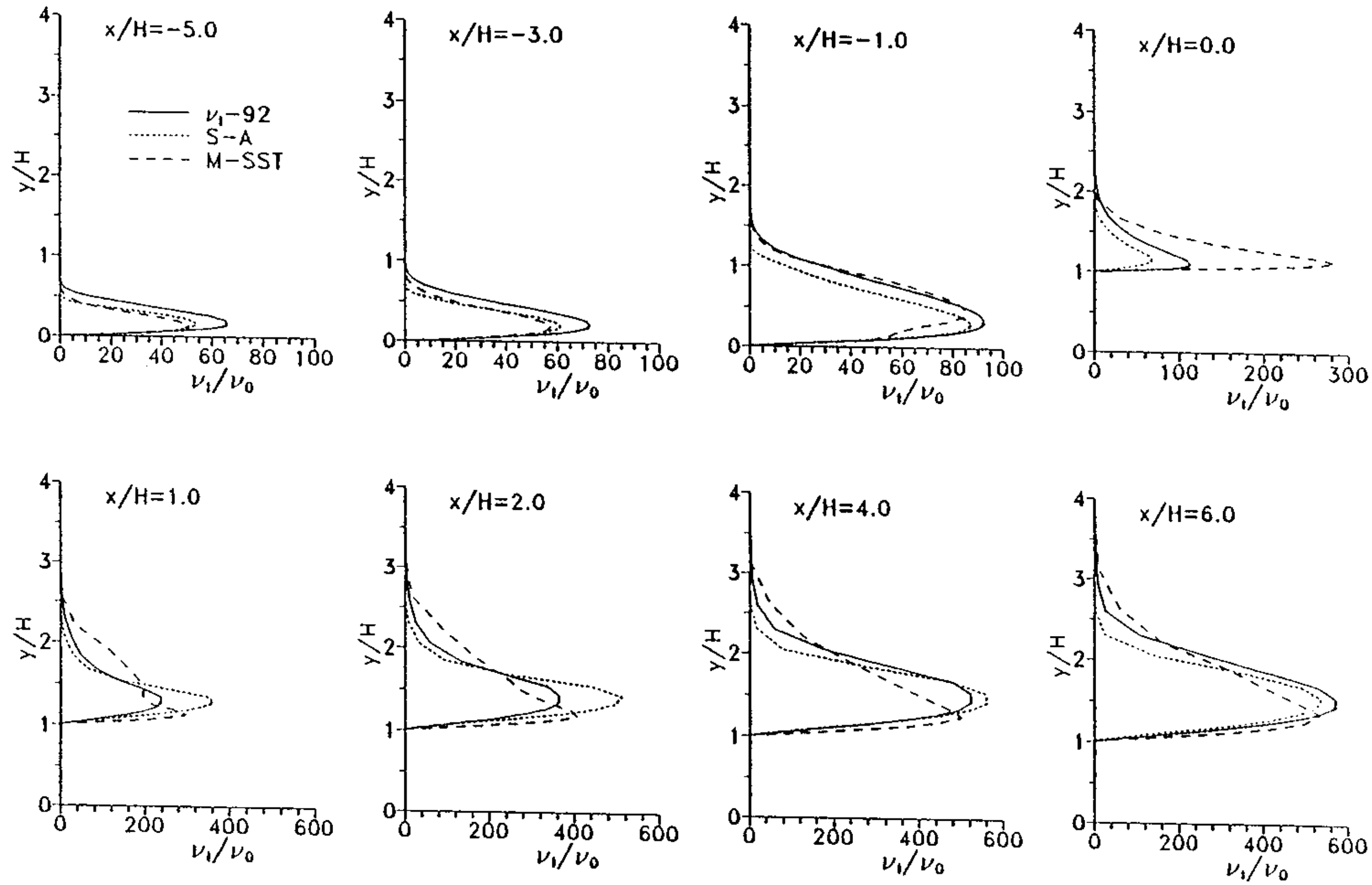

Figure 30. Eddy viscosity profiles for the M&B forward-facing step flow

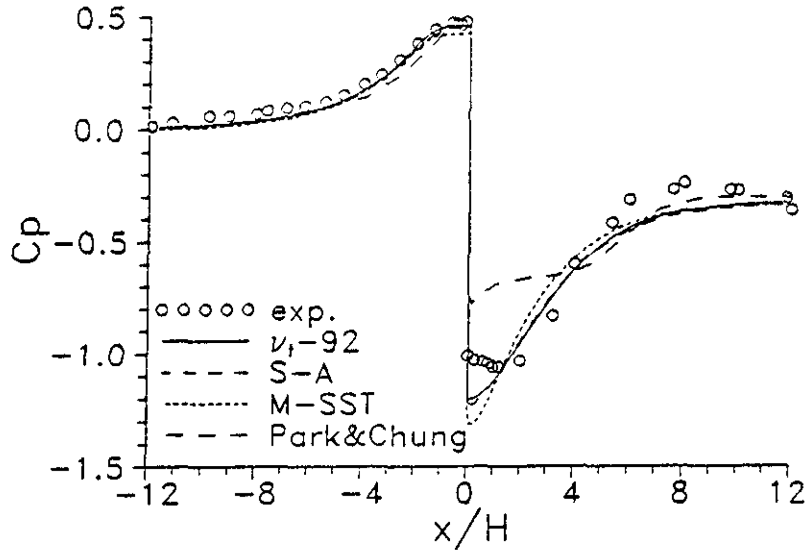

Figure 31. Pressure coefficient distribution along the step-side wall for the M&B flow

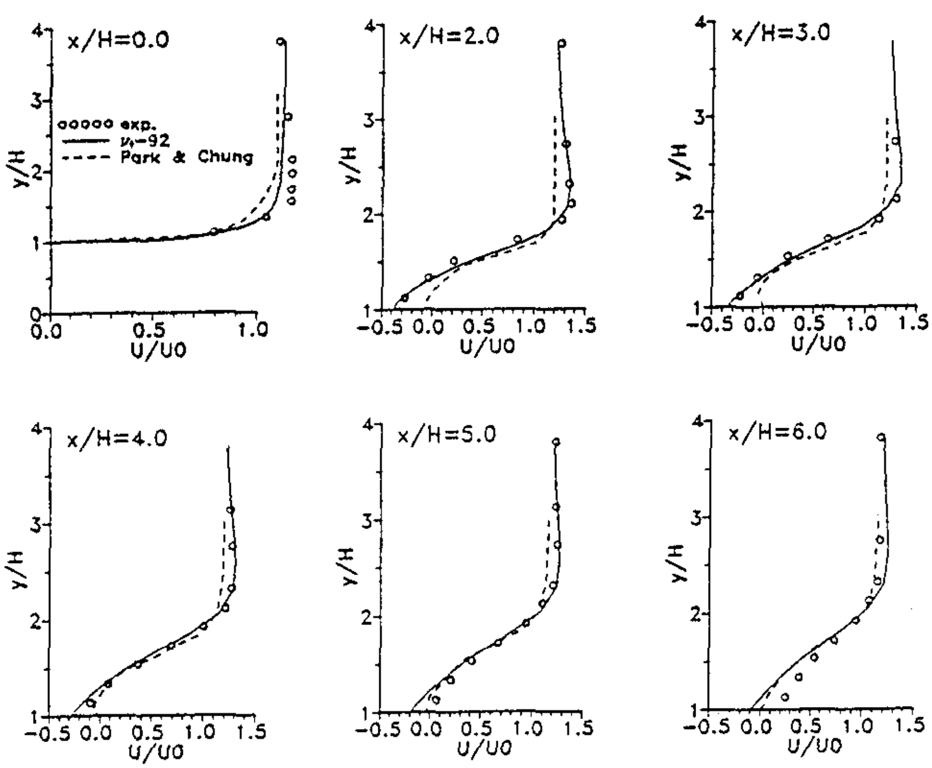

Figure 32. Comparison of velocity profiles for the M&B flow predicted by the ν_t-92 and by the k-ε model [28]

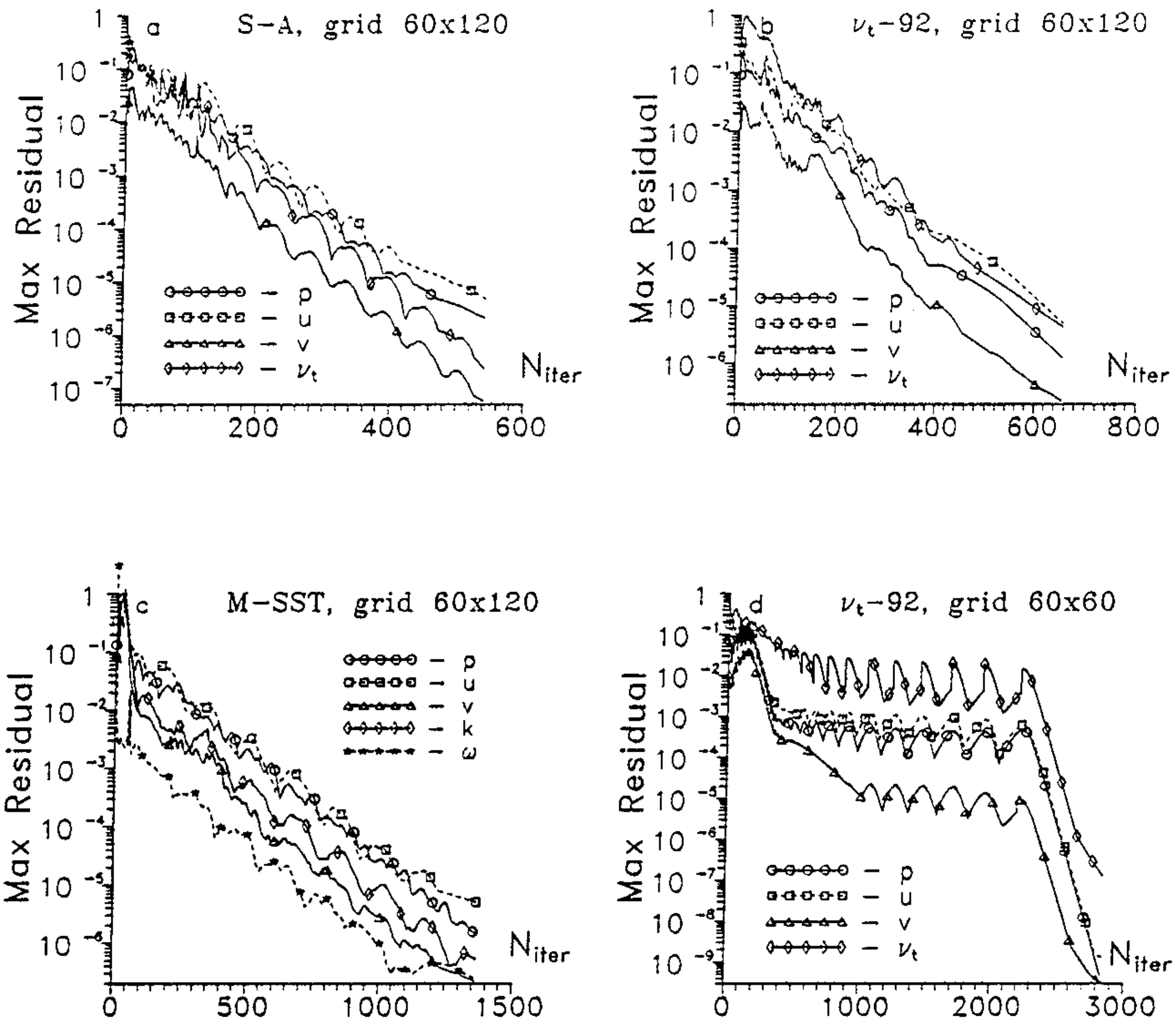

Figure 33. Convergence histories for the J&D, case 1, flow

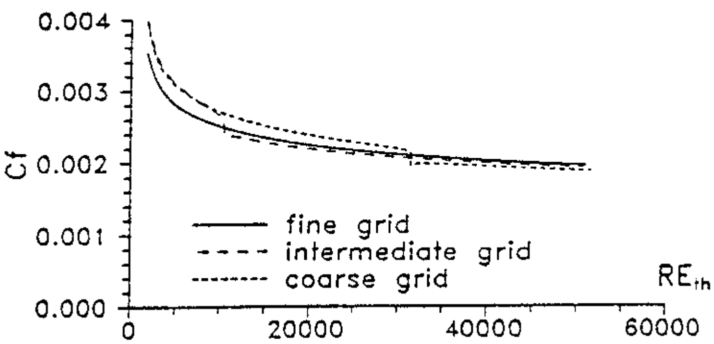

Figure 34. Effect of Y-grid coarsening on the flat plate skin friction predicted by the ν_t-92 model